iScience

Article

HSV-1 alters lipid metabolism and induces lipid droplet accumulation in functionally impaired mouse dendritic cells

Graphical abstract

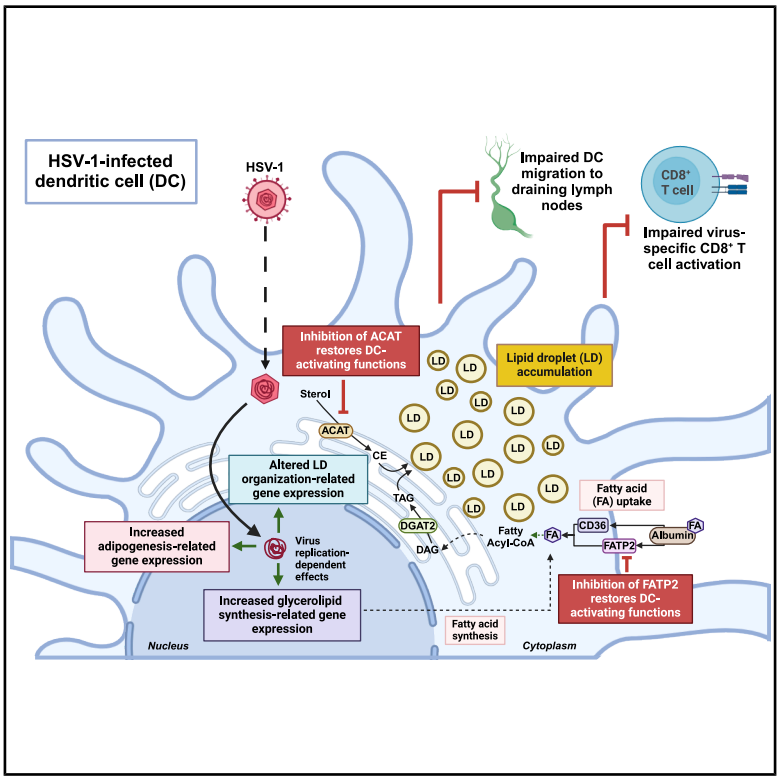

Highlights

- HSV-1 infection alters the expression of lipid metabolism genes and lipids in DCs
- HSV-1-infected DCs accumulate lipid droplets (LDs)
- Inhibition of lipid metabolism enzymes in HSV-1-infected DCs restores DC functions
- Targeting lipid metabolism enzymes in HSV-1-infected DCs elicits virus-specific CD8$^+$ T cells

Authors

Mónica A. Farías, Felipe A. Cancino, Areli J. Navarro, ..., Susan M. Bueno, Alexis M. Kalergis, Pablo A. González

Correspondence

pagonzam@uc.cl

In brief

Natural sciences; Biological sciences; Biochemistry; Immunology; Microbiology; Cell biology

Farías et al., 2025, iScience *28*, 112441
May 16, 2025 © 2025 The Authors. Published by Elsevier Inc.
https://doi.org/10.1016/j.isci.2025.112441

CellPress

iScience

CellPress
OPEN ACCESS

Article

HSV-1 alters lipid metabolism and induces lipid droplet accumulation in functionally impaired mouse dendritic cells

Mónica A. Farías,[1,2] Felipe A. Cancino,[1,2] Areli J. Navarro,[1,2] Luisa F. Duarte,[1,2,9] Abel A. Soto,[1,2] Eduardo I. Tognarelli,[1,2] Maximiliano J. Ramm,[3] Bárbara N. Alarcón-Zapata,[3] José Cordero,[2] Sergio San Martín,[4] Cristian Agurto-Muñoz,[4] Angello Retamal-Díaz,[1,5,6] Claudia A. Riedel,[1,7] Nelson P. Barrera,[2] Luis Bustamante,[3] Susan M. Bueno,[1,2] Alexis M. Kalergis,[1,2,8] and Pablo A. González[1,2,10,*]

[1]Millennium Institute on Immunology and Immunotherapy, Chile
[2]Facultad de Ciencias Biológicas, Pontificia Universidad Católica de Chile, Santiago, Chile
[3]Departamento de Análisis Instrumental, Facultad de Farmacia, Universidad de Concepción, Concepción, Chile
[4]Grupo Interdisciplinario de Biotecnología Marina (GIBMAR), Centro de Biotecnología, Universidad de Concepción, Concepción, Chile
[5]Departamento de Biotecnología, Facultad de Ciencias del Mar y de Recursos Biológicos, Universidad de Antofagasta, Antofagasta, Chile
[6]Centro de Investigación en Inmunología y Biotecnología Biomédica de Antofagasta, Hospital Clínico Universidad de Antofagasta, Antofagasta, Chile
[7]Centro de Investigación para la Resiliencia a Pandemias, Facultad Ciencias de la Vida, Universidad Andrés Bello, Santiago, Chile
[8]Departamento de Endocrinología, Facultad de Medicina, Escuela de Medicina, Pontificia Universidad Católica de Chile, Santiago, Chile
[9]Present address: Centro de Medicina Regenerativa, Facultad de Medicina, Clínica Alemana, Universidad del Desarrollo, Santiago, Chile
[10]Lead contact
*Correspondence: pagonzam@uc.cl
https://doi.org/10.1016/j.isci.2025.112441

SUMMARY

Herpes simplex virus type 1 (HSV-1) significantly impairs dendritic cell (DC) function, ultimately eliciting the death of these cells. Here, we sought to assess whether HSV-1 modulates lipid metabolism in mouse DCs as a mechanism of immune evasion. For this, we performed RT-qPCR gene arrays with ingenuity pathway analysis (IPA), RNA sequencing (RNA-seq) and gene set enrichment analysis (GSEA), confocal microscopy, transmission electron microscopy, ultra-high-performance liquid chromatography-quadrupole time-of-flight (UHPLC-QTOF) analysis, pharmacological inhibition of eight lipid-metabolism-related enzymes in HSV-1-infected DCs, co-cultures between virus-specific transgenic $CD4^+$ and $CD8^+$ T cells and HSV-1-infected DCs, and *in vivo* assays with mice. We found that HSV-1 significantly alters lipid metabolism in DCs and induces lipid droplet (LD) accumulation in these cells. Pharmacological inhibition of two particular lipid metabolism enzymes was found to partially restore DC function. Overall, these results suggest that lipid metabolism plays an important role in the impairment of DC function by HSV-1.

INTRODUCTION

Herpes simplex virus type 1 (HSV-1) is a highly prevalent pathogen in humans that elicits lifelong infections by establishing latency in neurons from where it can reactivate and produce recurrent lesions.[1,2] Besides infecting epithelial cells and neurons,[3] HSV-1 also infects dendritic cells (DCs), key immune cells that initiate and regulate antiviral immunity.[4] HSV-1 significantly alters DC function by interfering with crucial processes such as maturation, viral antigen presentation on major histocompatibility complex class I (MHC-I) molecules,[4–6] autophagosome flux, migration to lymph nodes, as well as T cell activation.[7,8] HSV-1 infection of DCs also induces apoptosis.[4] Interestingly, most of the processes that are negatively modulated by HSV-1 in DCs can be prevented by inhibiting the unfolded protein response (UPR) inositol-requiring enzyme-1α (IRE-1α)/X-box-binding protein-1 (XBP-1) axis in these cells upon infection[6,9] or by promoting the expression of the host enzyme heme oxygenase-1 (HO-1).[10]

On the other hand, lipid droplets (LDs) are neutral lipid-rich organelles mainly composed of triglycerides (TAGs) and cholesterol esters (CEs).[11] However, LDs may also contain other lipids such as diglycerides (DAGs), cholesterol, acylceramides (acylCer), retinyl esters, and fat-soluble vitamins, among others.[12–14] Although LDs are predominantly related to energy reservoirs within some types of cells, such as hepatocytes and adipocytes, they have also been reported to modulate viral infections, contribute to immune regulation, and participate in UPR cellular responses.[15–17]

Importantly, LDs in DCs have been associated with reduced antigen presentation to T cells, mainly due to reduced MHC-I expression on the surface of DCs.[17] Consistently, LDs with oxidized and truncated lipids in tumor-associated DCs have also been reported to interact with MHC-I, hampering the

This is an open access article under the CC BY-NC-ND license (http://creativecommons.org/licenses/by-nc-nd/4.0/).

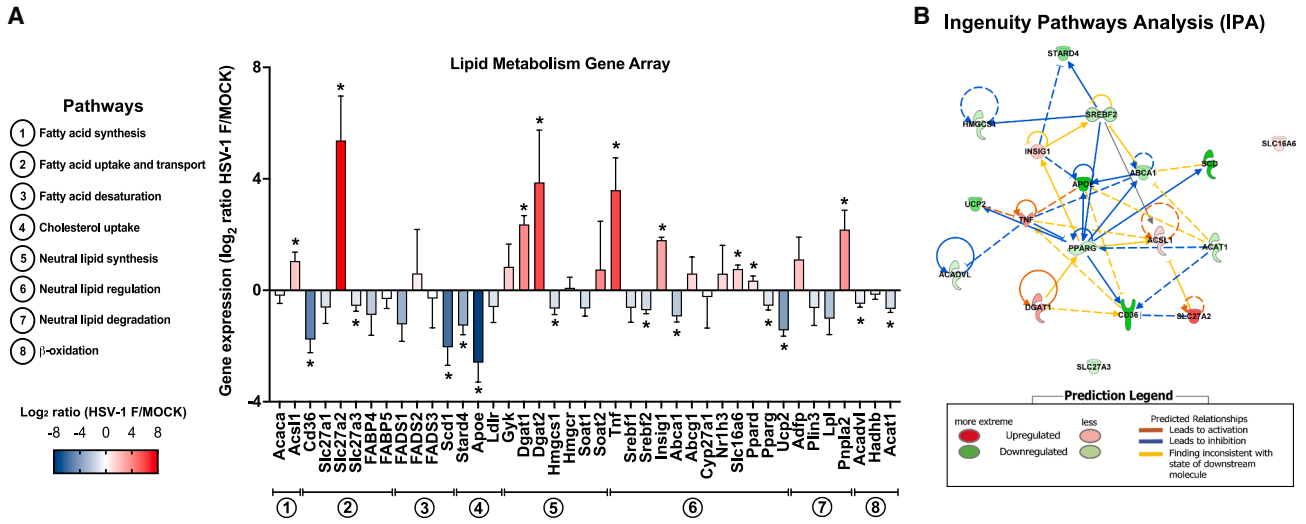

Figure 1. HSV-1 modulates neutral-lipid-metabolism-related gene expression in BMDCs

(A) Neutral-lipid-metabolism-related gene expression in BMDCs infected with HSV-1 strain F at MOI 3 12 hpi. Data were standardized using the $2^{-(\Delta\Delta Ct)}$ method based on the mRNA levels of the *Gapdh* housekeeping gene and after normalization based on the $\log_2$ ratio of the uninfected BMDCs (MOCK-treated samples). (B) Ingenuity pathway analysis (IPA) network diagram of genes associated with neutral lipid metabolism in BMDCs infected with HSV-1 that are significantly modulated at 12 hpi. Data in (A) show means ± SEM of three independent assays. The statistical analyses were performed using two-way ANOVA and Bonferroni multiple comparisons test. (*$p < 0.05$).

See also Figure S1, Tables S1 and S2.

stimulation of $CD8^+$ T cell response.[18,19] However, inhibition of fatty acid (FA) synthesis in DCs has been shown to reduce the dendropoiesis of DCs in the liver and lymphoid organs in mice.[20] FA inhibition also reduced MHC-I expression, increased the production of interleukin-12 (IL-12) and monocyte chemoattractant protein-1 (MCP-1) proinflammatory cytokines, and promoted the activation of $CD4^+$ and $CD8^+$ T cells and the induction of a DC-mediated cytotoxic T lymphocyte response, indicating that lipid metabolism can have profound effects over the function of DCs.[20]

Recently, HSV-1 was reported to induce LD formation in astrocytes early during infection (8 h), with LDs playing an antiviral effect in these cells as a cellular mechanism for restricting HSV-1 genome replication at early stages of infection.[21] In epithelial cells (COS-7 cells), glycoprotein D (gD) of HSV-1 was found to interact with the host protein viperin, colocalizing with LDs and the Golgi apparatus.[22] However, this report did not show evidence that HSV-1 induces the formation of LDs in this cell type.[22]

HSV-1 also modulates the synthesis of lipids involved in cell signaling processes in epithelial cells, such as phosphoinositides, by increasing 4,5-phosphatidylinositol bisphosphate (PIP2) and decreasing 4-phosphatidylinositol (PIP).[23] Further, HSV-1 infection has been reported to induce the *de novo* synthesis of phospholipids in epithelial cells to produce new viral particles through the kinase activity of the viral protein Us3.[24–26] Finally, cholesterol, which is an essential component of cell membranes, has been reported to be required for numerous processes related to HSV-1 infection and replication cycle, such as virus entry, replication, the release of infectious particles, and cell-to-cell spread among epithelial cells (Vero cells) and fibroblasts.[27]

Because DCs play key roles in initiating and regulating antiviral immune responses and that lipid accumulation in these cells can impair their function, we sought to assess whether HSV-1 modulates lipid metabolism and LD accumulation in functionally impaired DCs. Importantly, we found that infection of these cells with HSV-1 elicits significant changes in neutral lipid metabolism and induces LD accumulation, which likely interferes with their function contributing to immune evasion by this virus.

RESULTS

HSV-1 modulates neutral-lipid-metabolism-related gene transcript levels in DCs

To assess whether HSV-1 infection modulates neutral-lipid-metabolism-related gene expression in DCs, first we performed an RT-qPCR gene array analysis focused on genes involved in pathways associated with (1) FA synthesis, (2) FA uptake and transport, (3) FA desaturation, (4) cholesterol uptake, (5) neutral lipid synthesis, (6) neutral lipid regulation, (7) neutral lipid degradation, and (8) neutral lipid degradation mediated by β-oxidation (see Figure S1A). As shown in Figure 1A, mRNA transcripts of genes related to each of these lipid-metabolism-related processes, except for β-oxidation, were significantly altered upon HSV-1 infection in DCs. The complete list of lipid metabolism enzymes related to these genes is detailed in Table S1. To evaluate the relationship between mRNA and protein expression, we measured the protein levels of four of the most significantly altered mRNA transcripts related to the aforementioned lipid metabolism processes: cluster of differentiation 36 (CD36), fatty acid transport protein 2 (FATP2), diacylglicerol O-acyltransferase 2 (DGAT2), and tumor necrosis factor α (TNF-α). While

some mRNAs correlated with their corresponding protein levels (*Slc27a2* and *Tnf*), others did not (*Cd36* and *Dgat2*), likely due to the multiple levels of regulation that exist between DNA transcription and mRNA translation within the cell (see Figures S1B and S1C).

To evaluate the interaction network of the genes whose mRNA transcripts were evaluated in the RT-qPCR gene array described earlier, particularly those that were significantly modulated between HSV-1-infected DCs and MOCK-treated control DCs, we performed ingenuity pathway analysis (IPA). This bioinformatic tool allows assessing high-throughput data in the context of biological systems (Figure 1B). Most genes within the output network generated were related to each other through non-canonical interactions, suggesting novel interactions among the analyzed genes associated with neutral lipid metabolism in the context of DC infection by HSV-1. However, these unexpected pathways may also occur to some extent because of reduced correlation between mRNA and protein levels for certain lipid-metabolism-related genes and proteins (see Table S2). Noteworthy, the gene *Slc16a6* did not show any direct interactions with other neutral lipid metabolism genes in the array, likely because its function is particularly related to the transport of monocarboxylates such as lactate, pyruvate, and ketone bodies (Figure 1B).

RNA-seq analyses suggests altered lipid-metabolism-related pathways in HSV-1-infected DCs

To extend the above-mentioned findings, we performed RNA-seq analyses of HSV-1-infected DCs recovered 12 h post-infection (hpi) compared with MOCK-treated DCs (see Figure S1D). Normalized read counts were used for carrying out gene set enrichment analysis (GSEA) to compare HSV-1-infected and MOCK-treated DC conditions using Reactome, Gene Ontology, and Wikipathways databases (Figure 2A).[28–31] The output GSEA interaction networks showed a significant number of enriched gene sets related to catabolic lipid processes that were negatively regulated, such as β-oxidation (see Figures S1E and S1F; Table S3A), and pathways related to FA synthesis (Figure 2A). However, HSV-1-infected DCs also positively regulated two sets of genes associated with anabolic lipid processes, adipogenesis, and glycerolipids and glycerophospholipids (Figure 2A).

A more detailed analysis of the GSEA related to adipogenesis, as well of the subset of genes related to this process displayed in the form of a heatmap, showed important differences in mRNA abundance for a considerable number of genes in HSV-1-infected DCs as compared to the MOCK control, which were either significantly upregulated or downregulated upon infection (see Figures 2B–2E; Table S3B). Similar results were observed for the GSEA related to glycerolipids and glycerophospholipids, key pathways in the synthesis of TAGs (see Figures 2C–2F; Table S3C). Furthermore, a GSEA related to LD organization was importantly upregulated in HSV-1-infected DCs when compared to MOCK-treated cells, although the differences were not statistically significant ($p = 0.053$) (see Figures 2D–2G; Table S3D). However, as seen in the corresponding heatmap, the expression of many of the genes within the subset were significantly altered. On the other hand, a GSEA directly related to LD formation did not show differences between HSV-1-infected and MOCK-treated DCs (see Figures S1G and S1H; Table S3E). A leading-edge analysis of the most significantly modulated genes in lipid-associated processes in HSV-1-infected DCs revealed that the highest represented gene in the adipogenesis subset analysis was *Acsl5* (Acyl-CoA synthetase long-chain family member 5), which was represented in 14 gene subsets (see Figure S1I). The second most represented gene linked to adipogenesis-related routes was *Acadm* (Acyl-CoA dehydrogenase medium chain), which was represented in 10 gene subsets (see Figure S1J). For the process related to LD organization, the genes *Cds1* (CDP-diacylglycerol synthase 1), *Pla2g4c* (phospholipase A2 group IVC), *Fitm1* (fat storage inducing transmembrane protein 1), and *Rnf213* (ring finger protein 213) were found to be the most represented, each found in two subsets (see Figure S1H).

Overall, these results indicate that HSV-1 induces significant changes in the expression of lipid-metabolism-related genes in DCs, which can be related to reduced lipid catabolism processes, as well as increased expression of genes associated with adipogenesis, and glycerolipid and glycerophospholipid processes. These effects may alter the levels and types of lipids existing in these cells upon HSV-1 infection, which could translate into the accumulation of saturated FAs and neutral lipids within these cells, namely in the form of LDs.

HSV-1-infected DCs accumulate lipid droplets

Lipid droplet formation in the endoplasmic reticulum (ER) and its expansion into the cytoplasm is characterized by the accumulation of neutral lipids in organelle-like structures within the cell that can be detected using neutral lipid probes. Using such types of probes, we measured by flow cytometry neutral lipid levels in HSV-1 strain F-infected DCs at 12 and 18 hpi (Figures 3A and 3B). We found that although at 12 hpi HSV-1-infected DCs did not display an increase in neutral lipid levels (Figure 3A), at 18 hpi this accumulation was significant when compared to MOCK-treated DCs (Figure 3B). Next, we analyzed neutral lipid accumulation in DCs by confocal microscopy. We found that HSV-1-infected DCs displayed significant amounts of LD structures at 12 and 18 hpi when compared to MOCK-treated cells or DCs inoculated with HSV-1-UV-inactivated virus (Figure 3C). Microscopy analyses of these LDs revealed that the number of LDs per cell (Figure 3D), and their size (Figure 3E), were significantly higher in DCs infected with HSV-1 MOI 3.0 at 12 and 18 hpi when compared to controls. To assess if the induction of LDs in HSV-1-infected DCs depended on the strain of HSV-1 used, we additionally performed confocal microscopy analyses using HSV-1 strains KOS and 17syn$^+$ (see Figures S2A and S2B). HSV-1 strain 17syn$^+$ elicited a significant increase in the numbers of LDs at 12 hpi, similar to the results obtained with HSV-1 strain F (see Figures S2C and S2D), and significant changes in the area of LDs were observed at 12 and 18 hpi (see Figures S2E and S2F). On the other hand, HSV-1 KOS elicited a significant increase in LD size at 18 hpi (see Figure S2E). Furthermore, we analyzed the accumulation of LDs in HSV-1-strain-F-infected DCs using transmission electron microscopy (TEM) at 12 and 18 hpi (Figure 3F). As observed in-Figure 3F, a significant increase in the number of non-electron-dense structures that can be related to LDs could be detected

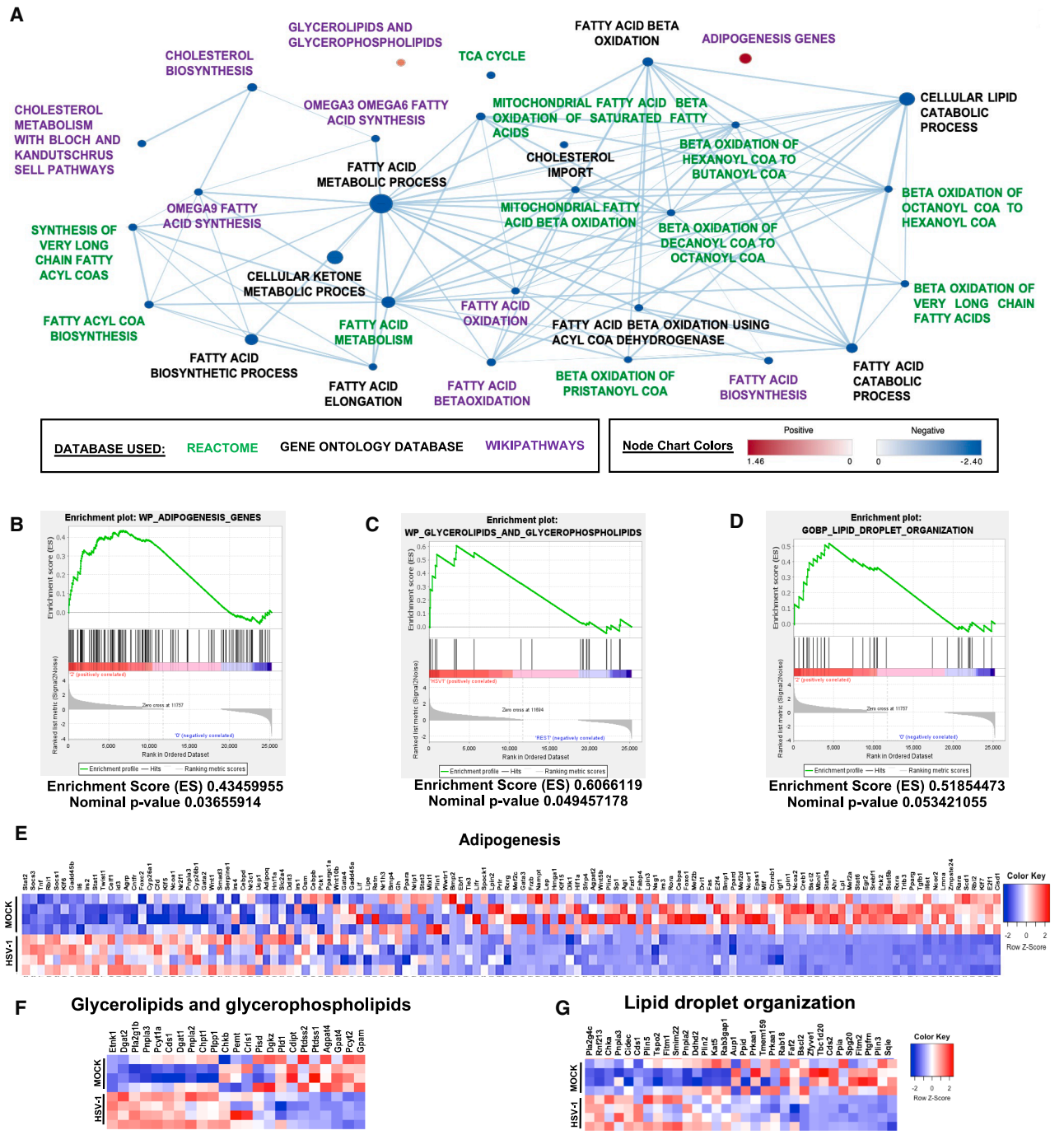

Figure 2. HSV-1 modulates neutral-lipid-metabolism-related gene set enrichments in BMDCs

(A) Network of lipid-metabolism-related processes significantly modulated in HSV-1 strain F-infected-DCs at MOI 3 12 hpi determined by RNA-seq. Multiple databases were used: Reactome (green), Gene Ontology database (black), and Wikipathways (purple). Access the network in an interactive manner using the following URL link: https://www.ndexbio.org/#/network/5c9c2021-bcdb-11ef-99aa-005056ae3c32. Enrichment plots and heatmaps for (B and E) adipogenesis-, (C and F) glycerolipids-and-glycerophospholipids-, and (D–G) lipid-droplet-organization-related genes. GSEA: normalized RNA counts obtained after RNA-seq were compared with the Gene Ontology database. The green line represents the enrichment score, and vertical black lines show hits enriched in HSV-1-infected (red) or MOCK-treated (blue) DCs ($n = 4$). The statistical analyses were performed using two-way ANOVA and Bonferroni multiple comparisons test. For the GSEA, the statistical test used was Kolmogorov-Smirnov (*$p < 0.05$).

See also Figure S1 and Table S3.

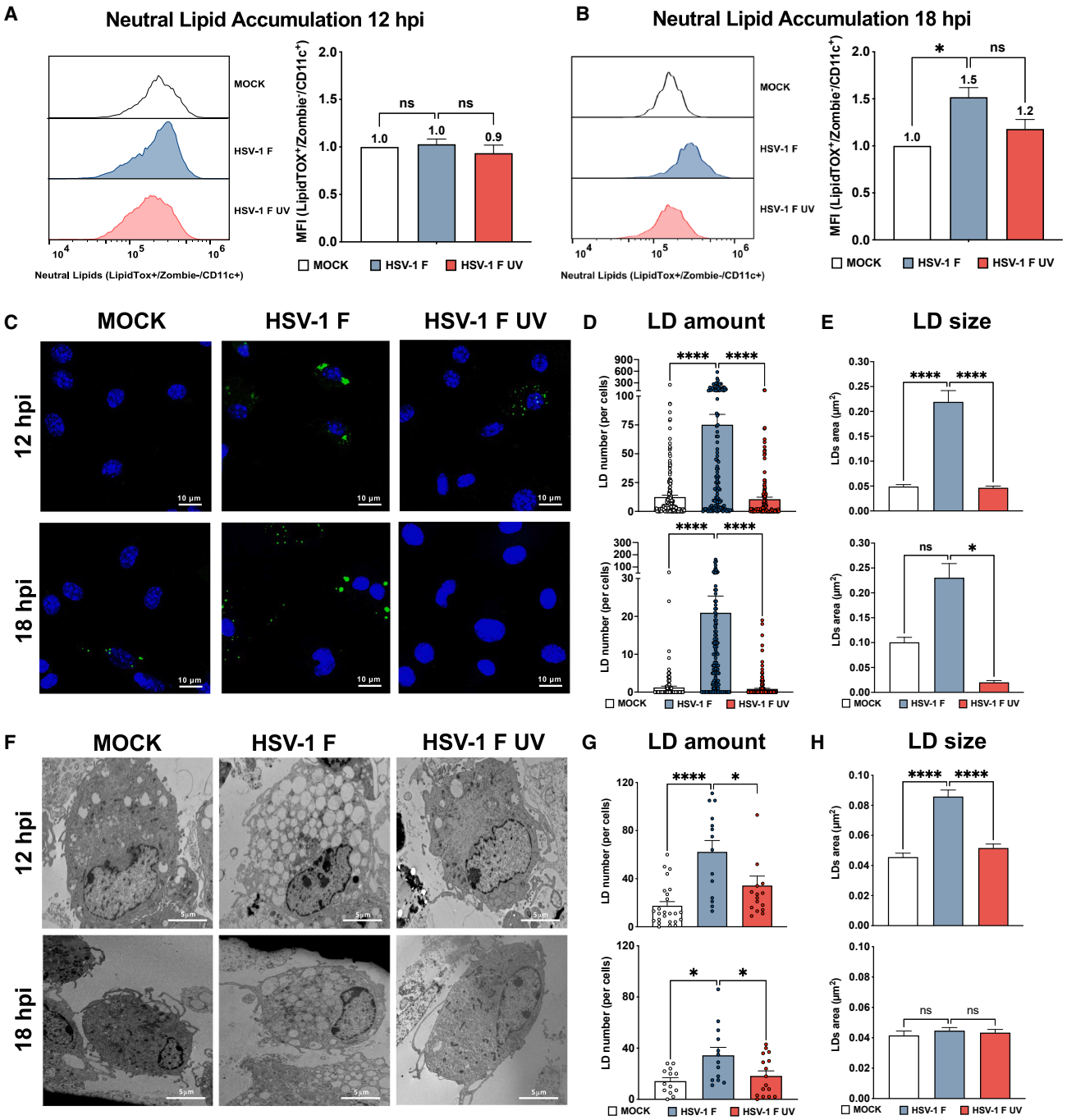

Figure 3. HSV-1 induces lipid droplet accumulation in BMDCs

Total neutral lipid levels were measured by flow cytometry in live DCs (HCS LipidTOX$^+$/CD11c$^+$/Zombie$^-$ cells), infected with HSV-1 strain F at MOI 3, either (A) 12 hpi or (B) 18 hpi.

(C) Confocal microscopy at 100X of neutral lipids using the neutral lipid probe BODIPY 493/503 in DCs infected with HSV-1 at 12 hpi (upper panels) or 18 hpi (lower panels). Scale bars: 10 µm.

(D) LD number and (E) LD size determined by confocal microscopy using a neutral lipid probe BODIPY 493/503 in DCs infected with HSV-1 at 12 hpi (upper panels) or 18 hpi (lower panels).

(F) Transmission electron microscopy at 4,200X of DCs infected with HSV-1 at 12 hpi (upper panels) or 18 hpi (lower panels). Scale bars: 5 µm.

(G) LD number and (H) LD size determined by TEM in DCs infected with HSV-1 at 12 hpi (upper panels) or 18 hpi (lower panels). Analyses show means ± SEM of three independent assays. Statistical analyses were performed using two-way ANOVA and Bonferroni multiple comparisons test (*$p < 0.05$, ****$p < 0.0001$, ns: no statistical significance).

See also Figure S2.

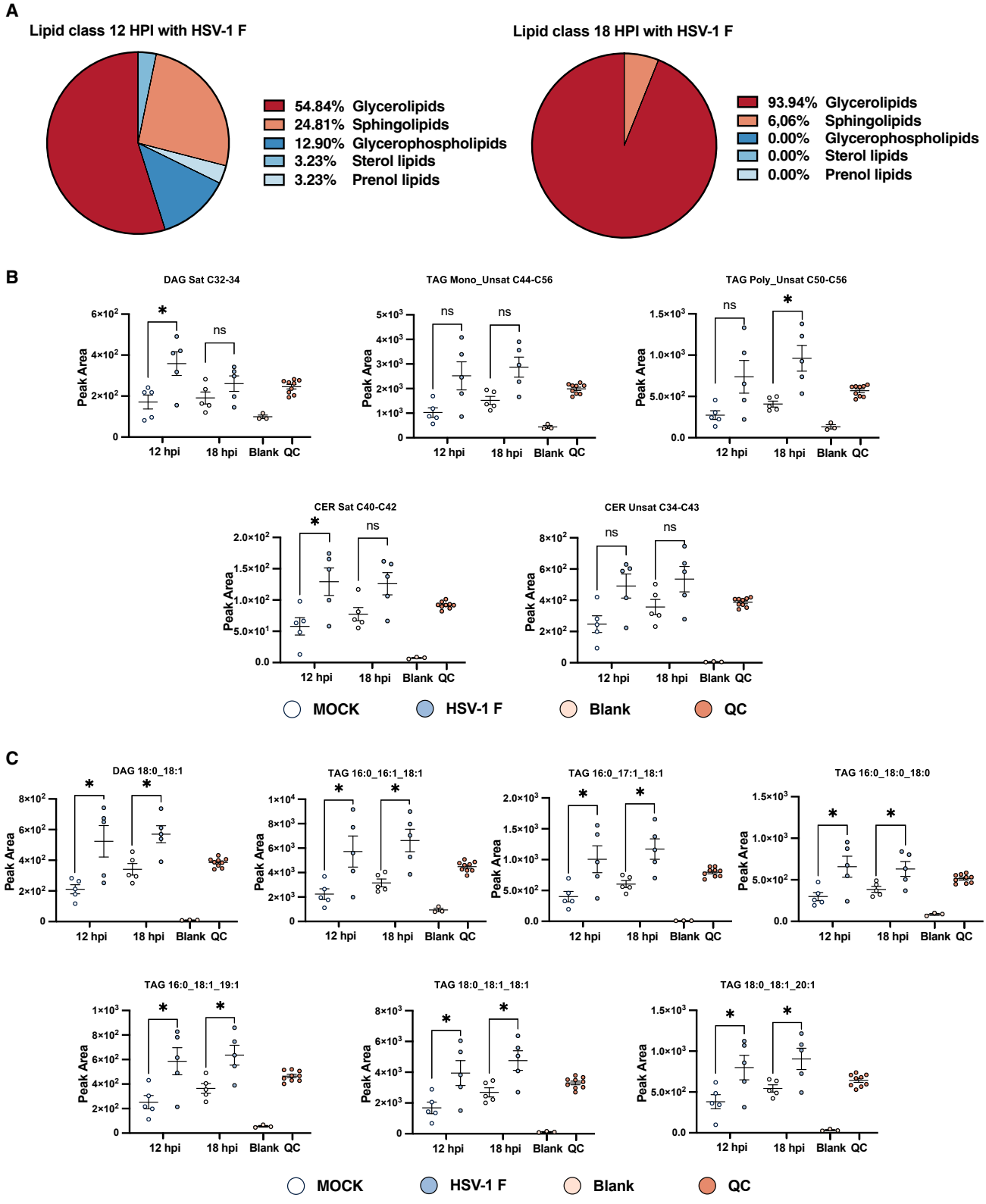

(legend on next page)

in these cells. An analysis of the number of these structures per cell (Figure 3G), and their size (Figure 3H), evidenced a significant increase of both parameters in HSV-1-infected DCs as compared to MOCK-treated DCs and DCs inoculated with HSV-1-UV-inactivated at 12 hpi, and for LD number at 18 hpi (Figure 3G). Noteworthy, the results obtained upon treatment with HSV-1-UV-inactivated suggest that LD accumulation in HSV-1-infected DCs depends on the viral replication cycle rather than structural viral components.

Because neutral lipid accumulation in HSV-1-infected DCs may be mediated by lipid uptake or *de novo* neutral lipid synthesis in these cells, we assessed the contribution of extracellular lipid uptake in neutral lipid accumulation. For this, we performed flow cytometry using a fluorescently labeled palmitic-acid-based probe. In this scenario, we did not observe any significant changes in the uptake of this lipid in HSV-1-infected DCs as compared to control DCs (see Figures S2G and S2H). Additionally, we evaluated the contribution of FA uptake by FA transport proteins (FATPs) and the FA translocase CD36 using pharmacological inhibitors for these receptors (lipofermata and sulfosuccinimidyl oleate [SSO], respectively). As shown in Figure S2H, inhibition of FATP significantly reduced FA uptake in MOCK-treated DCs and HSV-1-infected DCs, yet the inhibitor of CD36 only reduced FA uptake in MOCK-treated DCs and not HSV-1-infected DCs (see Figure S2H).

Taken together, these results suggest that DC infection with HSV-1 induces LD formation in these cells, which is likely mediated by *de novo* neutral lipid synthesis or the reorganization of existing lipids within infected DCs, a phenomenon that depended on an intact virus replication cycle.

HSV-1 alters the composition of lipids within infected DCs

Given that HSV-1 infection of DCs induces neutral lipid accumulation and the formation of LDs, we sought to analyze the composition of the lipids present within these cells. For this, we carried out ultra-high-performance liquid chromatography-quadrupole time-of-flight mass spectrometry (UHPLC-QTOF-MS) to identify predominant lipids produced in HSV-1-infected DCs compared with MOCK-treated cells (see Figures 4 and S3).

To detect lipid changes, we sought to perform an untargeted lipid analysis. The data integrity plots showed that the quality control (QC) pooled samples were grouped, suggesting low analytical variability compared to biological variability (see Figure S3A). A significantly larger lipid heterogeneity was observed in HSV-1-infected DCs as compared to MOCK-treated cells at 12 hpi ($p < 0.05$), which included glycerolipids, sphingolipids, glycerophospholipids, sterol lipids, and prenol lipids (Figure 4A). However, at 18 hpi, the lipids accumulating in a significant manner shifted toward glycerolipids, most of them TAGs (Figure 4A). A family analysis of the significantly accumulated lipid species at the analyzed time points showed that HSV-1 increased the abundance of saturated DAG (within 32–34 carbons, C32–34) at 12 hpi, polyunsaturated TAG (C50–56) at 18 hpi, as well as saturated ceramides (C40–42) at 12 hpi in virus-infected DCs as compared to MOCK-treated DCs (Figure 4B). Monounsaturated TAG and unsaturated ceramides (C44–56 and C34–43, respectively) were also modulated, although not significantly. At 12 hpi, we found a significant increase in saturated DAG and ceramides (see Figure 4B; Table S4). Consolidating both time points, we were able to detect eleven lipid subclasses II with a high confidence level (B), annotating 47 lipids, with 17 being significantly upregulated at 12 hpi, other 23 being significantly upregulated at 18 hpi, and 7 being significantly upregulated at both time points in HSV-1-infected DCs compared with MOCK-treated DCs (see Figure S3B). The seven lipids that were significantly upregulated at 12 and 18 hpi were all glycerolipids (Figure 4C).

Furthermore, using the Cytoscape software, we performed an interactome network with the representative lipid subclass upregulated in HSV-1-infected DCs and the corresponding results obtained in the RNA sequencing (RNA-seq) analysis compared to MOCK-treated DCs (see Figure S3C). Importantly, we found that the results obtained in our untargeted lipid approach agreed with the results of the RNA-seq analysis. Mainly, we found that lipids associated with glycerolipid, cholesterol, ceramides, and glycerophospholipids pathways correlated with elevated mRNA levels of genes associated with the corresponding anabolic pathways. In contrast, mRNA levels of genes associated with catabolic pathways were decreased in HSV-1-infected DCs (see Figure S3D). The remaining 40 lipids that were significantly regulated at either 12 or 18 h after HSV-1 infection are presented in Figure S4. Furthermore, the specific lipid species that were increased in HSV-1-infected DCs as compared to MOCK-treated DCs are outlined in the Table S5 for a more detailed analysis.

Overall, the lipidomic analysis indicates that HSV-1 infection of DCs elicits significant alterations in lipid composition related to neutral lipid homeostasis in these cells, and changes vary over time after the infection.

Inhibition of neutral-lipid-metabolism-related enzymes hinders HSV-1 replication in DCs

To assess the effects of neutral-lipid-metabolism-related enzymes over the replication of HSV-1 in DCs, we tested inhibitors of neutral lipid synthesis over the yield of infectious HSV-1 particles released from DCs, as well as the expression of three late viral proteins by western blot (i.e., gB, gD, and the virion protein 16 [VP16]) (Figure 5). Specifically, we assessed the effects of drugs that inhibit diacylglycerol O-acyltransferase 1 (DGAT1, using the drug A922500), DGAT2 (using the drug PF-06424439), and acyl-CoA: cholesterol acyltransferase 1 and 2 (ACAT1 and 2, using the drug avasimibe) (Figures 5A–5C). In parallel, we assessed

Figure 4. HSV-1 infection elicits significant lipid content changes in BMDCs

(A) Pie chart depicting the lipid classes significantly altered in BMDCs infected with HSV-1 strain F at MOI 3 12 hpi and 18 hpi.

(B) Boxplots of the sum of lipid classes detected in HSV-1-infected BMDCs at 12 and 18 hpi.

(C) Boxplots of specific lipid metabolites were detected in HSV-1-infected BMDCs at 12 hpi and 18 hpi ($n = 5$). The statistical analyses were performed using two-way ANOVA and Bonferroni multiple comparisons test (*$p < 0.05$, ns: no statistical significance).

See also Figure S3 and S4, Tables S4 and S5.

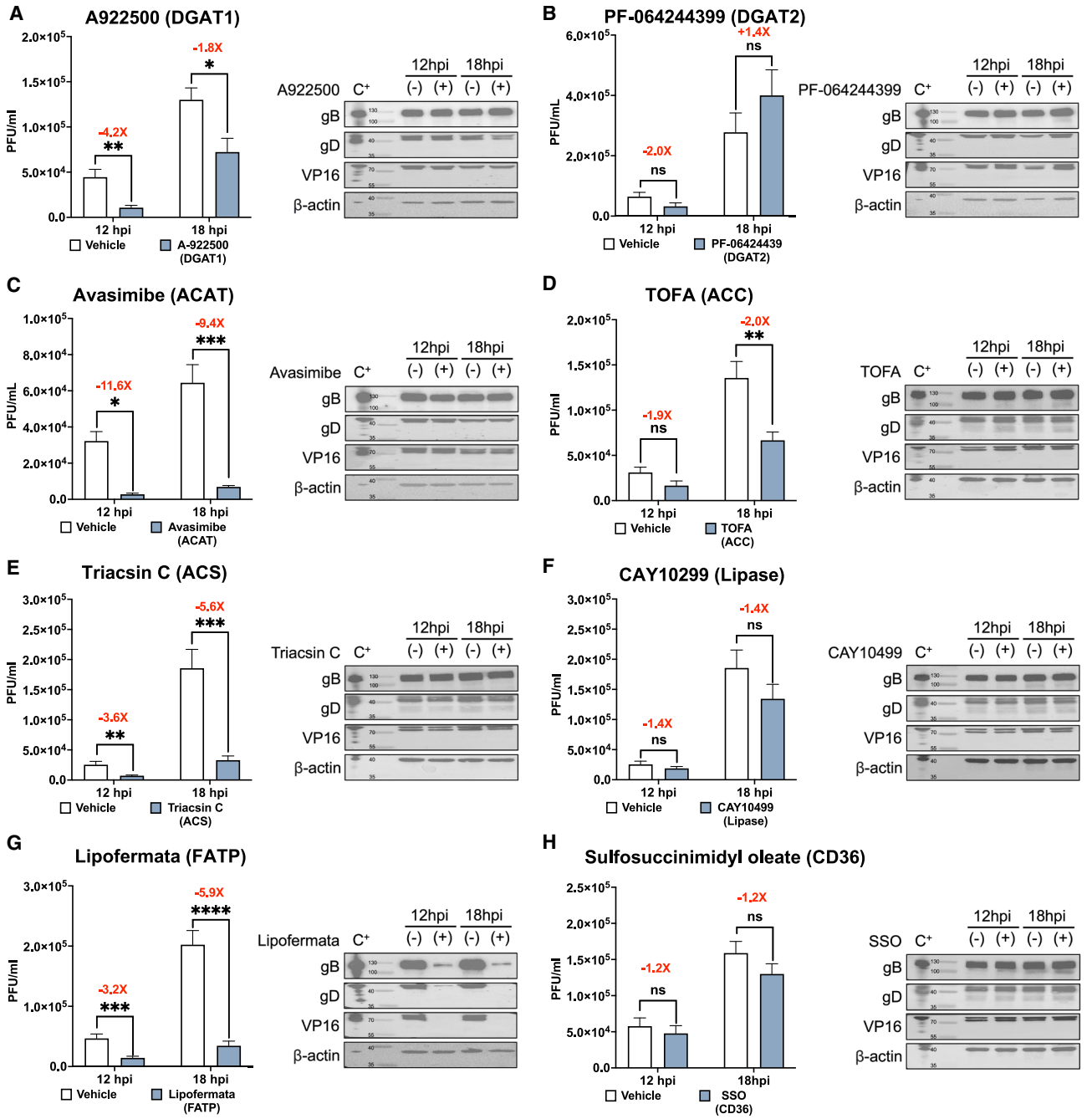

Figure 5. Yield of infectious HSV-1 and viral protein synthesis in BMDCs treated with inhibitors of lipid-metabolism-related enzymes

Plaque-forming units (PFUs) and viral protein expression analyses (western blot) of HSV-1 late viral proteins (glycoprotein B, glycoprotein D, and VP16) in BMDCs treated for 3 h with the (A) DGAT1 inhibitor A-922500 (10 μM) (B) DGAT2 inhibitor PF-06424439 (10 μM), (C) ACAT inhibitor avasimibe (10 μM), (D) ACS inhibitor TOFA (10 μM), (E) ACS inhibitor triacsin C (10 μM), (F) lipase inhibitor CAY10499 (10 μM), (G) FATP inhibitor lipofermata (10 μM), or (H) CD36 inhibitor sulfo-succinimidyl oleate (SSO, 50 μM) and then infected with HSV-1 strain F at MOI 3 for 12 hpi or 18 hpi. (–) corresponds to vehicle treatment (DMSO) and (+) to treatment with the inhibitor. C^+ corresponds to Vero-HSV-1-infected cells (positive control). The analyses shown are means ± SEM of three independent assays. The statistical analyses were performed using two-way ANOVA and Bonferroni multiple comparisons test (*$p < 0.05$, **$p < 0.01$, ***$p < 0.001$, ****$p < 0.0001$, ns: no statistical significance).

See also Figure S5.

the impact of these drugs over LD formation in the context of viral infection and found that all the drugs assessed reduced LD formation in HSV-1-infected DCs when compared to vehicle-treated HSV-1-infected cells (see Figures S5A–S5C). HSV-1-infected DCs treated with the DGAT1 or ACAT inhibitors, but not the DGAT2 inhibitor, reduced the output of infectious viral particles at 12 and 18 hpi (Figures 5A–5C) without an evident impact over viral protein expression (see Figures 5A–5C and S5D–S5F). These results suggest that TAG-synthesis-related metabolic pathways mediated by DGAT1 and CE synthesis, through ACAT, play relevant roles in the replication cycle of HSV-1, altogether affecting LD formation in the context of infection.

Moreover, we found that inhibition of FA synthesis through the inhibition of acetyl-CoA carboxylase (ACC) with 5-(tetradecycloxy)-2-furancarboxylic acid (TOFA) or acetyl-CoA synthetase (ACS) with triacsin C also elicited a reduction in infectious virus output (Figures 5D and 5E), as well as reduced LD formation (see Figures S5A–S5C), but did not elicit significant changes over the expression of the viral proteins assessed (see Figures 5D, 5E, S5G, and S5H). These results suggest that the initial steps involved in the synthesis and activation of FAs are not directly involved in the corresponding phases of the HSV-1 replication cycle, namely late viral protein synthesis, but do impact later processes related to virus output in DCs.

Furthermore, we sought to explore if the degradation of LDs affected the replication cycle of HSV-1 in DCs. For this, we inhibited the enzymatic activity of lipases that degrade neutral lipids in LDs using the inhibitor CAY10499. Under this experimental condition, we observed an accumulation of LDs in HSV-1-infected CAY10499-treated DCs when compared to untreated HSV-1-infected DCs (see Figures S5A–S5C). Furthermore, when inhibiting lipases with CAY10499, no significant differences were observed regarding viral particle output or the expression of late viral proteins (see Figures 5F and S5i).

Finally, we assessed the impact of inhibiting FA uptake over the yield of infectious virus in the supernatants of the cells and viral protein expression. Inhibition of FATP-mediated FA uptake with lipofermata (which mainly inhibits FATP2) reduced infectious virus yield (Figure 5G), the expression of late viral proteins in DCs (see Figures 5G and S5J), as well as LD formation (see Figures S5A–S5C). On the other hand, the inhibition of CD36 with the drug SSO did not alter viral particle egress nor late viral protein expression (see Figures 5H and S5K), and overall increased LD formation in HSV-1-infected DCs, as compared to control DCs (Figures S5A–S5C). This finding is consistent with HSV-1 reducing the expression of the gene *Cd36* in infected DCs (Figure 1A).

Taken together, these results indicate that neutral-lipid-metabolism-related enzymes play important roles for the replication cycle of HSV-1 in DCs, with the most significant effects elicited by enzymes that are involved in FA and CE synthesis, namely DGAT1, ACAT, ACC, and ACS. Based on our findings, FA uptake mediated by FATP would also play a relevant role for the viral replication cycle.

Role of neutral-lipid-metabolism-related enzymes over the function of DCs upon HSV-1 infection

Because HSV-1 induces significant apoptosis in DCs at 24 hpi,[10,32,33] we sought to assess the impact of lipid-metabolism-related enzymes during infection over the viability of DCs and their function (Figure 6). Interestingly, we found that among the enzymes/proteins DGAT1, DGAT2, ACAT, ACC, ACS, lipase, FATP, and CD36, only inhibition of ACAT and FATP had significant impacts over DC viability upon HSV-1 infection (Figures 6C–6G). In contrast, inhibitors of other neutral-lipid-metabolism-related enzymes did not elicit any significant effects (Figure 6). Moreover, we assessed the contribution of these enzymes over the maturation of these cells. When analyzing the maturation profile of HSV-1-infected DCs treated with inhibitors of the enzymes indicated earlier, we did not observe any significant differences in the surface expression of total MHC-I or MHC-II molecules (see Figures S6A–S6H), nor the costimulatory molecules CD40, CD80, CD83, or CD86 (see Figures S6I–S6P), when compared to HSV-1-infected DCs that did not receive any drug.

Furthermore, to determine if the inhibition of certain neutral-lipid-metabolism-related enzymes restored relevant DC processes related to their functions, such as DC migration from the periphery (i.e., skin) to the corresponding draining lymph nodes, we measured the migration of CFSE-labeled DCs from the footpads of mice toward popliteal lymph nodes (pLNs).[6,34] For this, we assessed the migration of spleen-purified DCs that were first treated *in vitro* with ACAT or FATP inhibitors and infected with HSV-1 and then injected into the footpads of mice to assess their migration to the pLNs (Figure 7A). In this experiment, we observed that treating HSV-1-infected DCs with ACAT or FATP inhibitors elicited a significant increase in the number of DCs migrating to the pLNs as compared to vehicle-treated uninfected or vehicle-treated HSV-1-infected DCs (Figure 7B). As a positive control, DCs pulsed with activating stimuli, such as lipopolysaccharide (LPS) or Poly (I:C), promoted the migration of DCs to the corresponding LNs (see Figure S7C). Remarkably, avasimibe promoted the migration of adoptively transferred DCs to the pLN *per se*, regardless of infection, although in a non-significant manner (Figure 7B). Additionally, we performed an assay to determine the migration of endogenous DCs residing in the skin of hind footpads of mice to the corresponding pLNs after injecting ACAT or FATP inhibitors at this site with or without HSV-1 (Figure 7C). Noteworthy, we observed that both total DCs and dermal DCs, but not Langerhans cells, from the footpads of uninfected and HSV-1-infected mice treated with the ACAT avasimibe inhibitor migrated in significantly higher numbers from the skin to the pLNs when compared to vehicle-treated uninfected footpads or vehicle-treated HSV-1-infected footpads (Figures 7D–7F). The fact that the treatment with the ACAT inhibitor avasimibe increased the migration of total and dermal DCs from the skin to pLNs, regardless of infection, is unprecedented to our knowledge and deserves further analysis. This was not the case with the FATP inhibitor lipofermata, which did not significantly affect the migration of DCs to the LNs under this experimental setting (Figures 7D–7F).

Altogether, these results suggest that mainly CE synthesis and, to a lesser extent FATP activity, play important roles in the viability and migration of DCs from the skin to the draining lymph nodes upon HSV-1 infection and may impact the capacity of these DCs to present antigens to virus-specific T cells.

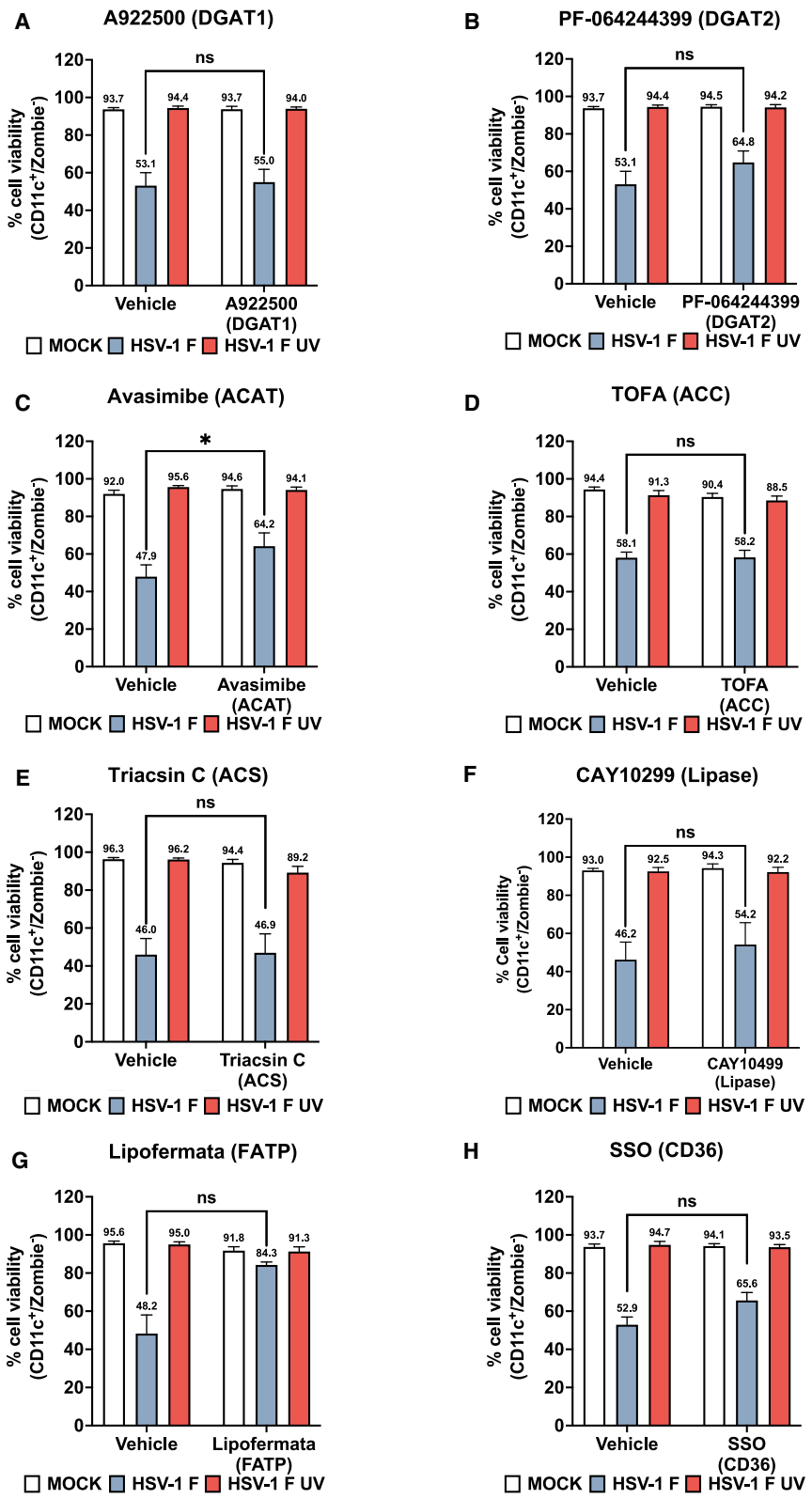

Figure 6. Inhibition of cholesterol ester synthesis (ACAT) or fatty acid uptake by fatty acid transport protein (FATP) recovers the viability of HSV-1-infected BMDCs

Flow cytometry analyses of BMDC viability (determined as $CD11c^+/Zombie^-$ cells) treated with (A) DGAT1 inhibitor A-922500 (10 μM), (B) DGAT2 inhibitor PF-06424439 (10 μM), (C) ACAT inhibitor avasimibe (10 μM), (D) ACS inhibitor TOFA (10 μM), (E) ACS inhibitor triacsin C (10 μM), (F) lipase inhibitor CAY10499 (10 μM), (G) FATP inhibitor lipofermata (10 μM), or (H) CD36 inhibitor sulfosuccinimidyl oleate (SSO, 50 μM) for 3 h, infected with HSV-1 strain F at MOI 3 for 1 h, and then further treated with the inhibitors for 17 h during infection. Vehicle treatment corresponds to the solvent used to dissolve the inhibitors (DMSO). The analyses shown are means ± SEM of three independent assays. The statistical analyses were performed using two-way ANOVA and Bonferroni multiple comparisons test ($*p < 0.05$, $**p < 0.01$, ns: no statistical significance).

See also Figures S6 and S7.

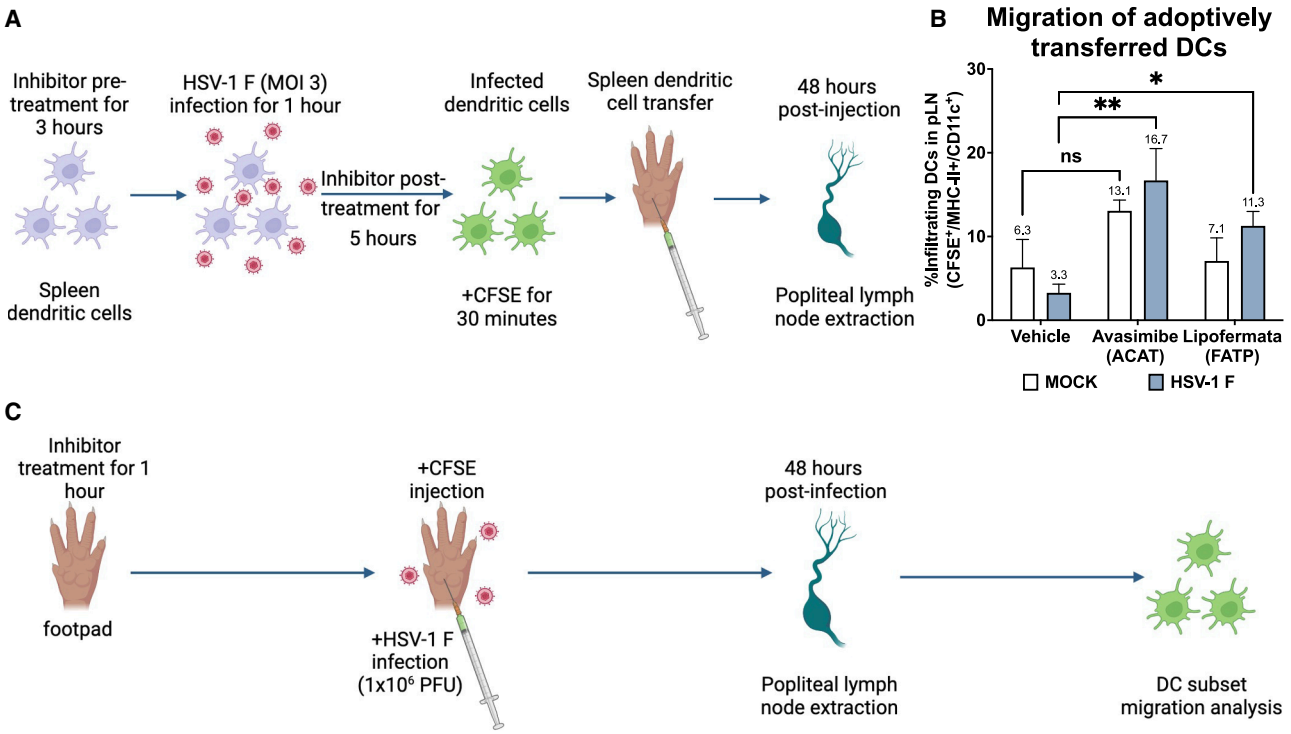

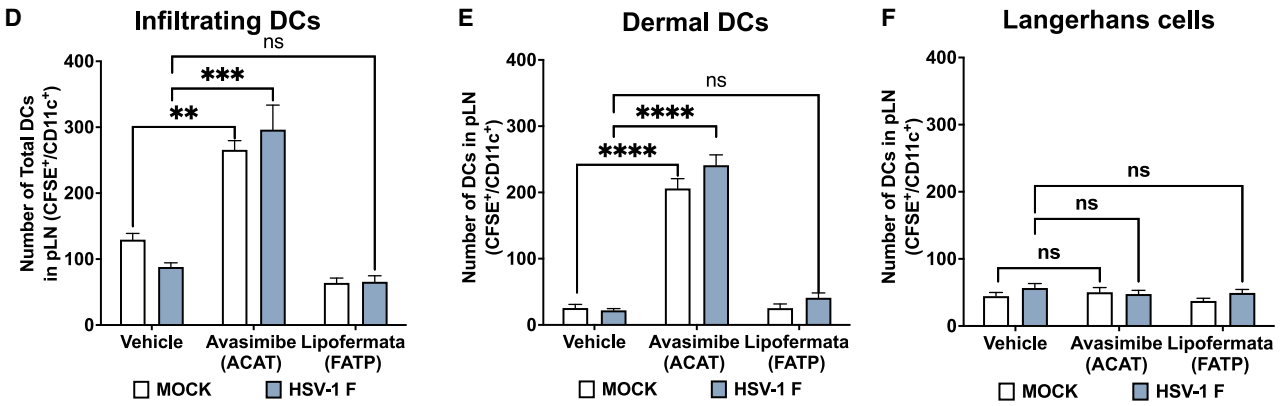

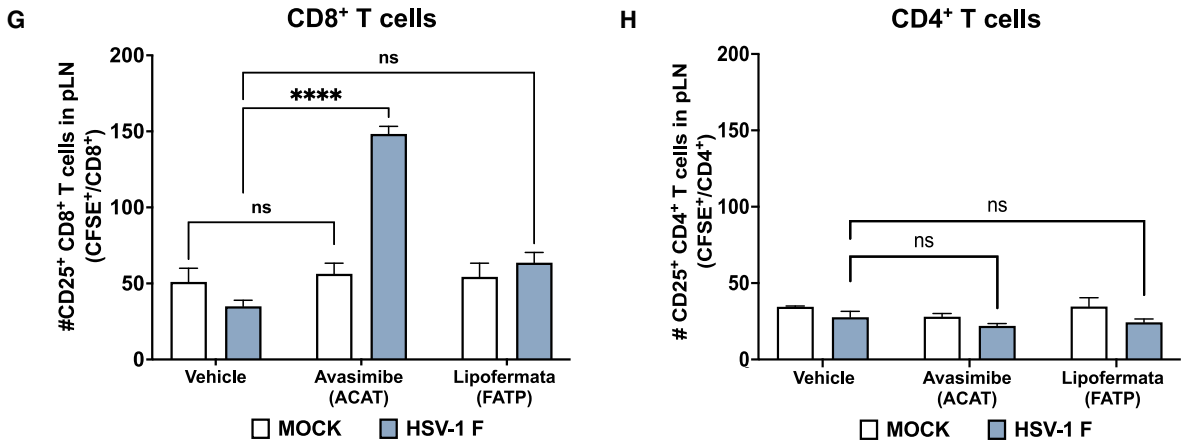

(legend on next page)

Finally, we sought to assess whether HSV-1-infected DCs treated with inhibitors of ACAT or FATP impact the activation of virus-specific $CD8^+$ and $CD4^+$ T cells *in vivo* (Figures 7G and 7H). For this, we used transgenic $CD8^+$ or $CD4^+$ T cells that recognize specific HSV viral peptide epitopes derived from gB and gD, presented on MHC-I and II molecules, respectively.[35,36] When the ACAT inhibitor avasimibe was injected into the footpads of mice together with HSV-1, we observed a significant increase in the number of activated virus-specific $CD8^+$ T cells expressing $CD25^+$ in the corresponding pLNs compared to vehicle-treated mice (Figure 7G). Because injection of avasimibe alone, without HSV-1, did not elicit the activation of virus-specific $CD8^+$ T cells, we conclude that the observed T cell activation upon treatment with avasimibe and HSV-1 injection is antigen-specific. On the other hand, when the FATP inhibitor lipofermata was injected into the footpads with or without HSV-1, no significant activation was observed for virus-specific $CD8^+$ T cells in the corresponding pLNs (Figure 7G). Regarding virus-specific $CD4^+$ T cells, we did not observe any significant differences in the expression of $CD25^+$ for any of the treatments (Figure 7H).

DISCUSSION

Previous studies report that infections with herpesviruses can elicit changes in cellular lipid synthesis.[21,37] Namely, HSV-1 has been described to increase the levels of lipids involved in cell signaling processes, such as phosphoinositides (PIs) in epithelial cells.[23,24] Varicella-zoster virus (VZV), another virus also belonging to the *Alphaherpesvirinae* subfamily, was reported to increase TAGs in fibroblasts,[37] and cytomegalovirus (CMV), which belongs to the *Betaherpesvirinae* subfamily, was shown to modulate cholesterol metabolism via the low-density lipoprotein (LDL)-receptor-related protein 1 also in fibroblasts.[38] Noteworthy, a recent study reported that HSV-1 can induce LD formation in astrocytes at early time points after infection, yet these structures were described to have antiviral effects in these cells.[21] Importantly, the effects of HSV-1 over lipid metabolism in DCs, which are key immune cells involved in initiating and regulating the host antiviral response, have not been reported to date, and relatively few studies describe neutral lipid alterations in DCs upon viral infection, none with HSV-1.[15,39–41]

Given that the dynamics and molecular mechanisms related to LD formation and their regulation in DCs are overall new to the field of immunometabolism, these processes may significantly differ from those currently reported in the literature, which mainly focuses on hepatocytes and adipocytes, where they were initially described.[42] Consistent with this notion, when comparing our findings with canonical metabolic predictions based on currently available datasets (i.e., IPA analysis), significant differences were observed regarding the predicted interaction networks for lipid metabolism genes modulated in the context of HSV-1 DC infection. Similarly, we observed that the GSEAs somewhat differed in some cases with our experimental data, particularly for LD formation and LD organization pathways, suggesting that these tools may need some adjustments to fit newly described LD-related processes in DCs, particularly in the context of viral interactions. However, as described in the results section, some discrepancies were identified between mRNA and protein levels for certain lipid-metabolism-related genes, likely stemming from the many regulatory steps occurring within the cell between gene transcription and mRNA translation. Therefore, the variations observed in the IPA and GSEA analyses in this study, compared to literature-based canonical pathways for lipid metabolism, should be interpreted with this in mind. Overall, assessing enzyme activity or the corresponding enzymatic products, as done in this study, provides a more reliable validation of the occurrence of a given metabolic pathway under the tested conditions.

Notably, our RNA-seq analysis revealed that the mRNA transcripts of *Acsl5* and *Acadm* were significantly downregulated in HSV-1-infected DCs compared to the MOCK control. Acyl-CoA synthetase long-chain family member 5 (ACSL5), the protein encoded by *Acsl5,* plays a key role in lipid metabolism and is involved in the production of long-chain fatty acids (LCFAs) for various processes, including lipogenesis. However, its role in the metabolism of DCs is unknown. *Acsl5* knockout in hepatic cells results in decreased TAG levels,[43] whereas *Acsl5*

Figure 7. Inhibition of ACAT in HSV-1-infected spleen DCs promotes enhanced migration of HSV-infected and non-infected DCs and the activation of the virus-specific $CD8^+$ T cells *in vivo*

(A) Schematic representation of the method used for assessing the migration of DCs to popliteal lymph nodes. DCs purified from the spleen were previously treated *in vitro* with the ACAT inhibitor avasimibe, FATP inhibitor lipofermata, or vehicle-treated for 3 h and then infected with HSV-1 strain F at MOI 3 for 6 h before injection into the footpads of mice.

(B) Flow cytometry analyses of the migration of the DCs treated as indicated above with the ACAT inhibitor avasimibe (10 μM), FATP inhibitor lipofermata (10 μM), or vehicle-treated from the skin of footpads to popliteal lymph nodes 48 h after injection (n = 3).

(C) Schematic representation of the method used to assess skin-resident DC migration from the skin to popliteal lymph nodes (pLNs). Footpads were treated with ACAT inhibitor avasimibe (10 μM), FATP inhibitor lipofermata (10 μM), or vehicle for 1 h and then inoculated with HSV-1 strain F.

(D) Flow cytometry analyses of total infiltrating DC migrating from the skin of footpads to popliteal lymph nodes 48 h after injection of the ACAT inhibitor avasimibe, FATP inhibitor lipofermata, or vehicle together with $1x10^6$ PFU HSV-1 strain F in the footpad with the tracking dye CFSE (the analysis was performed over $CFSE^+$/$MHC\text{-}II^+$/$CD11c^+$-gated cells).

(E) Quantification of infiltrating dermal DCs (dDCs; $CD207^+$/$CD103^+$/$MHC\text{-}II^+$/$CD11c^+$/$CFSE^+$ cells) and (F) infiltrating Langerhans cells (LCs, $CD207^+$/$CD103^-$/$MHC\text{-}II^+$/$CD11c^+$/$CFSE^+$ cells) relocating from the skin to the draining popliteal lymph nodes after footpad injection of the ACAT inhibitor, FATP inhibitor, or vehicle and infection with HSV-1 and the tracking dye CFSE.

(G) Surface expression of CD25 (T cell activation marker) in virus-specific gBT-I $CD8^+$ T cells or (H) gDT-II $CD4^+$ T cells obtained from popliteal lymph nodes of mice injected in the footpads with ACAT inhibitor avasimibe or FATP inhibitor lipofermata and then inoculated with HSV-1. A two-way ANOVA with the Bonferroni post-test was used. (n = 3 mice/group, $^*p < 0.05$, $^{***}p < 0.001$, $^{****}p < 0.0001$, ns: no statistical significance.

See also Figure S7.

knockdown in the same cells reduces LD formation. This reduction has been associated with decreased incorporation of oleic acid or acetic acid into intracellular TAGs, phospholipids, and cholesterol esters without altering lipogenic gene expression in hepatocytes.[44] These effects contrast with the results obtained herein, as we observed LD accumulation despite *Acsl5* transcripts being downregulated in HSV-1-infected DCs. Discrepancies could relate to the dynamics of *Acsl5* transcription, which may have dropped at the time point evaluated, or ACSL5 may have different roles in DCs than in hepatocytes. Noteworthy, ACSL5 deficiency in a tumor cell was reported to impair MHC-I presentation through the inhibition of the NOD-like receptor family CARD domain containing 5 (NLRC5) protein, which could relate to reduced T cell activation by HSV-1-infected DCs.[45] On the other hand, the *Acadm* gene encodes the medium-chain acyl-coenzyme A dehydrogenase (MCAD) enzyme, which catalyzes the initial step of mitochondrial medium-chain FA β-oxidation. Consistent with its role in this lipid degradation pathway, increased caveolin-1 expression in hepatocellular carcinoma cells has been reported to enhance the nuclear accumulation of sterol regulatory element-binding protein 1 (SREBP1), which suppresses *Acadm* transcription, leading to decreased β-oxidation and a consequent accumulation of fatty acids.[46] Although it should be determined experimentally, MCAD could also be playing a similar role herein in DCs.

Noteworthy, an increasing body of evidence reports lipid metabolism alterations in virus-infected DCs, which could contribute to better predictions regarding the effects of activated lipid metabolism pathways in infected cells. A recent report studying human monocyte-derived DCs (moDCs) infected with Zika virus found an enriched expression of genes related to lipid metabolism, which was mainly driven by a positive regulation of the sterol regulatory element-binding protein 2 (SREBP2) transcription factor and was found to have an impact on the activation of cholesterol biosynthesis and FA metabolism.[40] In our case, we observed that the mRNA transcript of *Srebf2* was significantly downregulated in HSV-1-infected DCs. On the other hand, infection of moDCs with the Japanese encephalitis virus (JEV) was reported to significantly downregulate the amount of transcripts related to peroxisome-proliferator-activated receptor (PPAR)/lipid biosynthetic pathways, as well as the regulation of sterol transport.[41] Interestingly, this downregulation of lipid metabolism was linked to an inflammatory response with increased levels of expression of TNF-α, MCP-1, and chemokine (C-C motif) ligand 5 (CCL5), as well as augmented levels of IL-6, IL-8, IL-10, and IL-12 during JEV infection.[41] In contrast to these reports, we mainly observed differences regarding the expression of genes related to the synthesis of TAGs, cholesterol, CE, and FA uptake. This suggests that viruses infecting DCs may elicit particular lipid metabolism fingerprints in these cells.

A recent study in mice and mouse embryonic fibroblasts (MEFs) reported that HSV-1 infection decreases the expression of the protein fatty acid desaturase 2 (FADS2), a protein involved in the synthesis of highly unsaturated fatty acids (HUFAs) from the essential polyunsaturated FA (PUFA) linoleic acid (LA) and alpha-linolenic acid (ALA), likely reflecting FADS2 activation and the accumulation of PUFA lipids upon infection.[47] In contrast to this report, we did not detect significant changes in *Fads2* gene expression in DCs infected with HSV-1, which highlights the existence of cell-type-specific viral effects, which we have observed in the past between DCs and epithelial cells.[9] However, it is important to note that antagonizing the effects of FADS2 in MEFs with shRNA or an FADS2 inhibitor (i.e., sc26196) decreased HSV-1 infection while treating the cells with 18-carbon PUFA ALA promoted the infection of MEFs.[47]

Reports studying the composition of neutral lipids in DCs in contexts other than viral infections indicate that these molecules significantly impact the function of these cells.[48] DCs obtained from tumors in mice and cancer patients have been described to have higher TAG levels than healthy individuals, which was accompanied by poor antigen presentation and limited T cell activation.[17,49] These results are consistent with our findings that suggest a negative role for LDs in HSV-1-infected DCs over T cell activation. Interestingly, activation of the IRE-1α pathway of the unfolded protein response has been reported to significantly modulate lipid content in DCs,[17] and thus, because this pathway impacts DC function during HSV-1 infection,[6,9] lipid alterations in these cells by HSV-1 may be mediated by this mechanism, which remains to be assessed. Considering the detrimental effects elicited by some lipids over DC function, it will be important to assess in more detail the characteristics of the specific lipids produced in DCs upon HSV-1 infection to better understand their specific roles in these cells in the context of infection. Importantly, PUFAs such as LA have been reported to promote apoptosis in human and murine DCs[50] and impair the maturation of DCs through a reduction in CD40, CD80, and CD86 expression, together with reduced IL secretion (IL-6 and IL-12p70), and a limited capacity to shift naive T cells toward T helper type 1 (Th1) and Th17 phenotypes.[50]

The most frequently studied pathogen relating to LD is hepatitis C virus (HCV),[51] with numerous inhibitors of lipid metabolism pathways showing effects over the replication cycle of this virus, such as TMP-153 (ACAT inhibitor) and triacsin C (ACS inhibitor), which reduce virus yield by decreasing virion assembly, without impacting significantly viral RNA synthesis.[52,53] On the other hand, avasimibe has been reported to inhibit the replication of hepatitis B virus (HBV),[54] HCV,[55] and severe acute respiratory syndrome coronavirus 2 (SARS-CoV-2),[56] and triacsin C as well as A922500 (DGAT1 inhibitor) were found to block SARS-CoV-2 replication.[57] Regarding herpesviruses, inhibitors of *de novo* FA biosynthesis, such as cerulenin, orlistat, and C75, have been shown to decrease the replication of VZV in human embryo fibroblast cells[58] and Epstein-Barr virus (EBV) in human epithelial tongue cells.[59] Based on these findings, it is possible that future antiviral drugs target some lipid-metabolism-related enzymes or processes to counteract infections and virus-related diseases. However, it is important to note that some studies report divergent effects for these inhibitors.[60,61]

Additionally, we found that inhibitors of FA and neutral lipid synthesis, as well as FA uptake elicited significant effects over the viability of HSV-1-infected DCs, their migration to draining lymph nodes, and their antigen-presenting capacity, which was evidenced in our *in vivo* assay. However, unexpectedly, we found that inhibition of ACAT in DCs or at the site of infection

in the skin elicited a significant increase in the migration of these cells to the draining LNs regardless of HSV-1 infection. Whether ACAT inhibition in cells neighboring the DCs in the skin may also promote DC migration to the pLNs remains to be determined experimentally. Interestingly, this DC-migration-promoting effect observed in our study upon ACAT inhibition by avasimibe may somewhat relate to the fact that ACAT1 inhibition is currently being tested as a means for treating head and neck cancer in mice with a DC-based vaccine.[62] Therefore, avasimibe could act as a DC-activating stimulus, such as LPS or Poly (I:C), although this remains to be experimentally assessed. Notably, a possible role for LPS or Poly (I:C) in LD accumulation in DCs is unknown. Moreover, avasimibe has been reported to improve DC targeting to induce HBV-specific T cytotoxic response.[63] In another report studying melanoma in mice, treatment with avasimibe increased plasma membrane cholesterol levels in $CD8^+$ T cells, which related to an enhanced immunological synapse, increased proliferation, and potentiated effector functions.[64] Additionally, simvastatin, a lipophilic statin that inhibits cholesterol synthesis by targeting 3-hydroxy-3-methylglutaryl coenzyme A (HMGCR), also has an adjuvant effect on DCs, with its effect attributed to the geranylgeranylation of small GTPases, including Rab5, resulting in increased antigen presentation to T cells, and T cell activation.[65] These results suggest that inhibiting the synthesis of cholesteryl esters with avasimibe may impact these latter upstream pathways, a phenomenon that requires further investigation. Finally, and noteworthy, the inhibition of ACAT in the footpads inoculated with HSV-1 promoted the activation of virus-specific $CD8^+$ T cells. Importantly, the activation of virus-specific $CD8^+$ T cells was antigen-specific, as it was only observed in the group receiving both avasimibe and HSV-1 and not in that receiving avasimibe only. Increased DC viability and DC migration to the draining LNs elicited by avasimibe treatment in the context of HSV-1 infection are likely key factors promoting the activation of these virus-specific $CD8^+$ T cells. Yet, why a similar effect was not induced over virus-specific $CD4^+$ T cells remains to be determined. It will also be relevant to assess whether the activation of virus-specific $CD8^+$ T cells alone may be sufficient for counteracting, to some extent, the effects of viral infection in infected animals.

Although our study considered well-reported inhibitors affecting lipid metabolism pathways, it is important to remember that some of these inhibitors may have broader and off-target effects. Therefore, it will be important to assess in future studies additional inhibitors, gene silencing approaches (e.g., siRNA or shRNA), or gene knock-out mutants (CRISPR) for a more profound understanding of the effects of HSV-1 infection over neutral lipid metabolism and impaired DC function.

Overall, in this study, we report a role for neutral-lipid-metabolism-related enzymes in the replication cycle of HSV-1 in DCs and lipid droplet accumulation in these cells upon infection with this virus. Further analyzing the lipids that are accumulated within the LDs in HSV-1-infected DCs and their specific roles during viral infection, as well as the role of the lipid-metabolism-related enzymes that are modulated during DC infection will likely shed light on potentially new approaches to limit HSV-1 evasion of the host adaptive immune response and promote effective antiviral immunity against this virus.

Limitations of the study

Some limitations of the study include the lack of proteomic analyses to validate the transcriptomic (RNA-seq) data, as significant differences can arise between mRNA transcript levels and protein levels due to the multiple regulatory steps of mRNA that occur between DNA transcription and mRNA translation. Another limitation is the relatively restricted set of drugs used to pharmacologically inhibit lipid-metabolism-related enzymes to assess their contribution to the altered lipid phenotype observed in HSV-1-infected DCs. Nevertheless, we assessed key enzymes involved in the most canonical lipid metabolism pathways, providing an initial framework for identifying lipid processes that may be linked to the observed phenotype in HSV-1-infected DCs.

RESOURCE AVAILABILITY

Lead contact

Further information and requests for resources and reagents should be directed to and will be fulfilled by the lead contact, Dr. Pablo A. González (pagonzam@uc.cl).

Materials availability

All mouse lines and materials used in this study were provided or purchased from the companies or researchers mentioned. This study did not generate any new or unique reagents.

Data and code availability

- RNA-seq data were deposited in the Gene Expression Omnibus database (GEO) under accession number GSE238169 and BioProject accession number PRJNA998087, available at the following URL: https://www.ncbi.nlm.nih.gov/geo/query/acc.cgi?acc=GSE238169. Lipidomic data were deposited in the Metabolights database under accession number MTBLS5163 and are available at the following URL: https://www.ebi.ac.uk/metabolights/editor/MTBLS5163/descriptors.
- This paper does not report original codes.
- Any additional information required for re-analyzing the data reported in this paper is available from the lead contact upon request.

ACKNOWLEDGMENTS

This work was funded/supported by the Agencia Nacional de Investigación y Desarrollo (ANID) – Millennium Science Initiative Program – Millennium Institute on Immunology and Immunotherapy (MIII) ICN2021_045 (former ICN09_016; P09/016-F), ANID FONDECYT Regular grants #1240971 (P.A.G.), #1231905 (S.M.B.), #1231851 (A.M.K.), ANID FONDECYT Iniciación grants #11241567 (L.F.D) and #11181200 (L.B.), and the Regional Government of Antofagasta through the Innovation Fund for Competitiveness FIC-R 2017 (BIP Code: 30488811-0). L.F.D. had an ANID FONDECYT Postdoctorado grant #3210473. M.A.F., F.A.C., E.I.T., A.J.N., and A.A.S. had/are ANID PhD fellows #21191390, #21251401, #21211300, #21241486, and #21241472, respectively. We are grateful to the Flow Cytometry Core Facility and the Advanced Microscopy Facility (UMA) at the Faculty of Biological Sciences of the Pontificia Universidad Católica de Chile, and Fondequip EQM 170023.

AUTHOR CONTRIBUTIONS

M.A.F. and P.A.G. designed experiments. M.A.F., F.A.C., A.J.N., L.F.D., E.I.T., B.N.A, A.R.D, and S.S.M. performed experiments. M.A.F., A.A.S., E.I.T., M.J.R., J.C., S.S.M., N.P.B., L.B., and P.A.G. analyzed the data. M.A.F., S.M.B., A.M.K., and P.A.G. wrote the manuscript. M.A.F., C.A.R., N.P.B., C.A.M., L.B., S.M.B., A.M.K., and P.A.G. edited the manuscript. All authors made significant contributions and revised the manuscript.

DECLARATION OF INTERESTS

The authors declare no competing interests.

STAR★METHODS

Detailed methods are provided in the online version of this paper and include the following:

- KEY RESOURCES TABLE
- EXPERIMENTAL MODEL AND STUDY PARTICIPANT DETAILS
  - Mice
  - Virus
  - Cell lines
  - Primary cell cultures
- METHOD DETAILS
  - DC infection with HSV-1
  - Pharmacological treatment of DCs
  - Lipid metabolism-related gene expression by RT-qPCR
  - Ingenuity pathway analysis (IPA)-RT-qPCR
  - Transcriptomic analyses of lipid metabolism-related genes
  - TNF-α cytokine detection
  - Neutral lipid measurements
  - Confocal microscopy
  - Transmission electron microscopy
  - Lipid uptake assay
  - Ultra-high performance liquid chromatography-quadrupole time-of-flight (UHPLC-QTOF) analysis
  - Plaque-forming unit assay
  - Western blot
  - Dendritic cell viability and maturation assay
  - DC migration and T cell activation *in vivo*
- QUANTIFICATION AND STATISTICAL ANALYSIS
  - RNA-seq gene set enrichment analyses
  - Statistical analyses

SUPPLEMENTAL INFORMATION

Supplemental information can be found online at https://doi.org/10.1016/j.isci.2025.112441.

Received: July 2, 2024
Revised: February 4, 2025
Accepted: April 10, 2025
Published: April 15, 2025

REFERENCES

1. Duarte, L.F., Carbone-Schellman, J., Bueno, S.M., Kalergis, A.M., Riedel, C.A., and González, P.A. (2025). Tackling cutaneous herpes simplex virus disease with topical immunomodulators-a call to action. Microbiol Rev. *38*, e0014724. https://doi.org/10.1128/cmr.00147-24.
2. Duarte, L.F., Reyes, A., Farías, M.A., Riedel, C.A., Bueno, S.M., Kalergis, A.M., and González, P.A. (2021). Crosstalk Between Epithelial Cells, Neurons and Immune Mediators in HSV-1 Skin Infection. Front. Immunol. *12*, 662234. https://doi.org/10.3389/fimmu.2021.662234.
3. Ibáñez, F.J., Farías, M.A., Retamal-Díaz, A., Espinoza, J.A., Kalergis, A.M., and González, P.A.. (2017). Pharmacological Induction of Heme Oxygenase-1 Impairs Nuclear Accumulation of Herpes Simplex Virus Capsids upon Infection. Front Microbiol *31*, 2108. https://doi.org/10.3389/fmicb.2017.02108.
4. Ma, F., Lf, D., Ei, T., and Pa, G. (2021). Herpes simplex virus interference with immunity: Focus on dendritic cells. Virulence *12*, 2583–2607. https://doi.org/10.1080/21505594.2021.1980990.
5. Wang, P., Kan, Q., Yu, Z., Li, L., Zhang, Z., Pan, X., and Feng, T. (2013). Recombinant adenovirus expressing ICP47 gene suppresses the ability of dendritic cells by restricting specific T cell responses. Cell. Immunol. *282*, 129–135. https://doi.org/10.1016/j.cellimm.2013.05.004.
6. Retamal-Diaz, A., Weiss, K.A., Tognarelli, E.I., Freire, M., Bueno, S.M., Herold, B.C., Jacobs, W.R., Jr., and Gonzalez, P.A. (2017). US6 Gene Deletion in Herpes Simplex Virus Type 2 Enhances Dendritic Cell Function and T Cell Activation. Front. Immunol. *8*, 1523. https://doi.org/10.3389/fimmu.2017.01523.
7. Gobeil, P.A.M., and Leib, D.A. (2012). Herpes simplex virus gamma34.5 interferes with autophagosome maturation and antigen presentation in dendritic cells. mBio *3*, e00267-12. https://doi.org/10.1128/mBio.00267-12.
8. Budida, R., Stankov, M.V., Döhner, K., Buch, A., Panayotova-Dimitrova, D., Tappe, K.A., Pohlmann, A., Sodeik, B., and Behrens, G.M.N. (2017). Herpes simplex virus 1 interferes with autophagy of murine dendritic cells and impairs their ability to stimulate CD8(+) T lymphocytes. Eur. J. Immunol. *47*, 1819–1834. https://doi.org/10.1002/eji.201646908.
9. Tognarelli, E.I., Retamal-Díaz, A., Farías, M.A., Duarte, L.F., Palomino, T. F., Ibañez, F.J., Riedel, C.A., Kalergis, A.M., Bueno, S.M., and González, P.A. (2021). Pharmacological Inhibition of IRE-1 Alpha Activity in Herpes Simplex Virus Type 1 and Type 2-Infected Dendritic Cells Enhances T Cell Activation. Front. Immunol. *12*, 764861. https://doi.org/10.3389/fimmu.2021.764861.
10. Tognarelli, E.I., Duarte, L.F., Farias, M.A., Cancino, F.A., Corrales, N., Ibanez, F.J., Riedel, C.A., Bueno, S.M., Kalergis, A.M., and Gonzalez, P.A. (2023). Heme Oxygenase-1 Expression in Dendritic Cells Contributes to Protective Immunity against Herpes Simplex Virus Skin Infection. Antioxidants *12*, 1170. https://doi.org/10.3390/antiox12061170.
11. Olzmann, J.A., and Carvalho, P. (2019). Dynamics and functions of lipid droplets. Nat. Rev. Mol. Cell Biol. *20*, 137–155. https://doi.org/10.1038/s41580-018-0085-z.
12. Samuel, A.Z., Miyaoka, R., Ando, M., Gaebler, A., Thiele, C., and Takeyama, H. (2020). Molecular profiling of lipid droplets inside HuH7 cells with Raman micro-spectroscopy. Commun. Biol. *3*, 372. https://doi.org/10.1038/s42003-020-1100-4.
13. Senkal, C.E., Salama, M.F., Snider, A.J., Allopenna, J.J., Rana, N.A., Koller, A., Hannun, Y.A., and Obeid, L.M. (2017). Ceramide Is Metabolized to Acylceramide and Stored in Lipid Droplets. Cell Metab. *25*, 686–697. https://doi.org/10.1016/j.cmet.2017.02.010.
14. Molenaar, M.R., Yadav, K.K., Toulmay, A., Wassenaar, T.A., Mari, M.C., Caillon, L., Chorlay, A., Lukmantara, I.E., Haaker, M.W., Wubbolts, R.W., et al. (2021). Retinyl esters form lipid droplets independently of triacylglycerol and seipin. J. Cell Biol. *220*, e202011071. https://doi.org/10.1083/jcb.202011071.
15. Farias, M.A., Diethelm-Varela, B., Navarro, A.J., Kalergis, A.M., and Gonzalez, P.A. (2022). Interplay between Lipid Metabolism, Lipid Droplets, and DNA Virus Infections. Cells *11*, 2224. https://doi.org/10.3390/cells11142224.
16. Bosch, M., Sanchez-Alvarez, M., Fajardo, A., Kapetanovic, R., Steiner, B., Dutra, F., Moreira, L., Lopez, J.A., Campo, R., Mari, M., et al. (2020). Mammalian lipid droplets are innate immune hubs integrating cell metabolism and host defense. Science *370*, eaay8085. https://doi.org/10.1126/science.aay8085.
17. Cubillos-Ruiz, J.R., Silberman, P.C., Rutkowski, M.R., Chopra, S., Perales-Puchalt, A., Song, M., Zhang, S., Bettigole, S.E., Gupta, D., Holcomb, K., et al. (2015). ER Stress Sensor XBP1 Controls Anti-tumor Immunity by Disrupting Dendritic Cell Homeostasis. Cellule *161*, 1527–1538. https://doi.org/10.1016/j.cell.2015.05.025.
18. Veglia, F., Tyurin, V.A., Mohammadyani, D., Blasi, M., Duperret, E.K., Donthireddy, L., Hashimoto, A., Kapralov, A., Amoscato, A., Angelini, R., et al. (2017). Lipid bodies containing oxidatively truncated lipids block antigen cross-presentation by dendritic cells in cancer. Nat. Commun. *8*, 2122. https://doi.org/10.1038/s41467-017-02186-9.
19. Ramakrishnan, R., Tyurin, V.A., Veglia, F., Condamine, T., Amoscato, A., Mohammadyani, D., Johnson, J.J., Zhang, L.M., Klein-Seetharaman, J., Celis, E., et al. (2014). Oxidized lipids block antigen cross-presentation

by dendritic cells in cancer. J. Immunol. *192*, 2920–2931. https://doi.org/10.4049/jimmunol.1302801.

20. Rehman, A., Hemmert, K.C., Ochi, A., Jamal, M., Henning, J.R., Barilla, R., Quesada, J.P., Zambirinis, C.P., Tang, K., Ego-Osuala, M., et al. (2013). Role of fatty-acid synthesis in dendritic cell generation and function. J. Immunol. *190*, 4640–4649. https://doi.org/10.4049/jimmunol.1202312.
21. Monson, E.A., Crosse, K.M., Duan, M., Chen, W., O'Shea, R.D., Wakim, L. M., Carr, J.M., Whelan, D.R., and Helbig, K.J. (2021). Intracellular lipid droplet accumulation occurs early following viral infection and is required for an efficient interferon response. Nat. Commun. *12*, 4303. https://doi.org/10.1038/s41467-021-24632-5.
22. Li, M., Liao, Z., Xu, Z., Zou, X., Wang, Y., Peng, H., Li, Y., Ou, X., Deng, Y., Guo, Y., et al. (2019). The Interaction Mechanism Between Herpes Simplex Virus 1 Glycoprotein D and Host Antiviral Protein Viperin. Front. Immunol. *10*, 2810. https://doi.org/10.3389/fimmu.2019.02810.
23. Langeland, N., Haarr, L., and Holmsen, H. (1986). Polyphosphoinositide metabolism in baby-hamster kidney cells infected with herpes simplex virus type 1. Biochem. J. *237*, 707–712. https://doi.org/10.1042/bj2370707.
24. Sutter, E., de Oliveira, A.P., Tobler, K., Schraner, E.M., Sonda, S., Kaech, A., Lucas, M.S., Ackermann, M., and Wild, P. (2012). Herpes simplex virus 1 induces de novo phospholipid synthesis. Virology *429*, 124–135. https://doi.org/10.1016/j.virol.2012.04.004.
25. Asher, Y., Heller, M., and Becker, Y. (1969). Incorporation of lipids into herpes simplex virus particles. J. Gen. Virol. *4*, 65–76. https://doi.org/10.1099/0022-1317-4-1-65.
26. Wild, P., de Oliveira, A.P., Sonda, S., Schraner, E.M., Ackermann, M., and Tobler, K. (2012). The herpes simplex virus 1 U(S)3 regulates phospholipid synthesis. Virology *432*, 353–360. https://doi.org/10.1016/j.virol.2012.06.020.
27. Wudiri, G.A., and Nicola, A.V. (2017). Cellular Cholesterol Facilitates the Postentry Replication Cycle of Herpes Simplex Virus 1. J. Virol. *91*, e00445-17. https://doi.org/10.1128/JVI.00445-17.
28. Fabregat, A., Sidiropoulos, K., Viteri, G., Forner, O., Marin-Garcia, P., Arnau, V., D'Eustachio, P., Stein, L., and Hermjakob, H. (2017). Reactome pathway analysis: a high-performance in-memory approach. BMC Bioinf. *18*, 142. https://doi.org/10.1186/s12859-017-1559-2.
29. Ashburner, M., Ball, C.A., Blake, J.A., Botstein, D., Butler, H., Cherry, J.M., Davis, A.P., Dolinski, K., Dwight, S.S., Eppig, J.T., et al. (2000). Gene ontology: tool for the unification of biology. The Gene Ontology Consortium. Nat. Genet. *25*, 25–29. https://doi.org/10.1038/75556.
30. Gene Ontology Consortium; Aleksander, S.A., Balhoff, J., Carbon, S., Cherry, J.M., Drabkin, H.J., Ebert, D., Feuermann, M., Gaudet, P., and Harris, N.L. (2023). The Gene Ontology knowledgebase in 2023. Gene *224*, iyad031. https://doi.org/10.1093/genetics/iyad031.
31. Agrawal, A., Balci, H., Hanspers, K., Coort, S.L., Martens, M., Slenter, D. N., Ehrhart, F., Digles, D., Waagmeester, A., Wassink, I., et al. (2023). WikiPathways 2024: next generation pathway database. Nucleic. Acids. Res. *52*, D679–D689. https://doi.org/10.1093/nar/gkad960.
32. Jones, C.A., Fernandez, M., Herc, K., Bosnjak, L., Miranda-Saksena, M., Boadle, R.A., and Cunningham, A. (2003). Herpes simplex virus type 2 induces rapid cell death and functional impairment of murine dendritic cells in vitro. J. Virol. *77*, 11139–11149. https://doi.org/10.1128/jvi.77.20.11139-11149.2003.
33. Bosnjak, L., Miranda-Saksena, M., Koelle, D.M., Boadle, R.A., Jones, C. A., and Cunningham, A.L. (2005). Herpes simplex virus infection of human dendritic cells induces apoptosis and allows cross-presentation via uninfected dendritic cells. J. Immunol. *174*, 2220–2227. https://doi.org/10.4049/jimmunol.174.4.2220.
34. Bollampalli, V.P., Nylen, S., and Rothfuchs, A.G. (2016). A CFSE-based Assay to Study the Migration of Murine Skin Dendritic Cells into Draining Lymph Nodes During Infection with Mycobacterium bovis Bacille Calmette-Guerin. J. Vis. Exp. *116*, 54620. https://doi.org/10.3791/54620.
35. Mueller, S.N., Heath, W., McLain, J.D., Carbone, F.R., and Jones, C.M. (2002). Characterization of two TCR transgenic mouse lines specific for herpes simplex virus. Immunol. Cell Biol. *80*, 156–163. https://doi.org/10.1046/j.1440-1711.2002.01071.x.
36. Bedoui, S., Whitney, P.G., Waithman, J., Eidsmo, L., Wakim, L., Caminschi, I., Allan, R.S., Wojtasiak, M., Shortman, K., Carbone, F.R., et al. (2009). Cross-presentation of viral and self antigens by skin-derived CD103+ dendritic cells. Nat. Immunol. *10*, 488–495. https://doi.org/10.1038/ni.1724.
37. Jerkofsky, M., and De Siervo, A.J. (1986). Differentiation of strains of varicella-zoster virus by changes in neutral lipid metabolism in infected cells. J. Virol. *57*, 809–815. https://doi.org/10.1128/JVI.57.3.809-815.1986.
38. Gudleski-O'Regan, N., Greco, T.M., Cristea, I.M., and Shenk, T. (2012). Increased expression of LDL receptor-related protein 1 during human cytomegalovirus infection reduces virion cholesterol and infectivity. Cell Host Microbe *12*, 86–96. https://doi.org/10.1016/j.chom.2012.05.012.
39. Avota, E., Gulbins, E., and Schneider-Schaulies, S. (2011). DC-SIGN mediated sphingomyelinase-activation and ceramide generation is essential for enhancement of viral uptake in dendritic cells. PLoS Pathog. *7*, e1001290. https://doi.org/10.1371/journal.ppat.1001290.
40. Branche, E., Wang, Y.T., Viramontes, K.M., Valls Cuevas, J.M., Xie, J., Ana-Sosa-Batiz, F., Shafee, N., Duttke, S.H., McMillan, R.E., Clark, A.E., et al. (2022). SREBP2-dependent lipid gene transcription enhances the infection of human dendritic cells by Zika virus. Nat. Commun. *13*, 5341. https://doi.org/10.1038/s41467-022-33041-1.
41. Chauhan, S., Rathore, D.K., Sachan, S., Lacroix-Desmazes, S., Gupta, N., Awasthi, A., Vrati, S., and Kalia, M. (2021). Japanese Encephalitis Virus Infected Human Monocyte-Derived Dendritic Cells Activate a Transcriptional Network Leading to an Antiviral Inflammatory Response. Front. Immunol. *12*, 638694. https://doi.org/10.3389/fimmu.2021.638694.
42. Napolitano, L., and Fawcett, D. (1958). The fine structure of brown adipose tissue in the newborn mouse and rat. J. Biophys. Biochem. Cytol. *4*, 685–692. https://doi.org/10.1083/jcb.4.6.685.
43. Luo, Q., Das, A., Oldoni, F., Wu, P., Wang, J., Luo, F., and Fang, Z. (2023). Role of ACSL5 in fatty acid metabolism. Heliyon *9*, e13316. https://doi.org/10.1016/j.heliyon.2023.e13316.
44. Bu, S.Y., and Mashek, D.G. (2010). Hepatic long-chain acyl-CoA synthetase 5 mediates fatty acid channeling between anabolic and catabolic pathways. J. Lipid Res. *51*, 3270–3280. https://doi.org/10.1194/jlr.M009407.
45. Lai, Y., Gao, Y., Lin, J., Liu, F., Yang, L., Zhou, J., Xue, Y., Li, Y., Chang, Z., Li, J., et al. (2024). Dietary elaidic acid boosts tumoral antigen presentation and cancer immunity via ACSL5. Cell Metab. *36*, 822–838. https://doi.org/10.1016/j.cmet.2024.01.012.
46. Ma, A.P.Y., Yeung, C.L.S., Tey, S.K., Mao, X., Wong, S.W.K., Ng, T.H., Ko, F.C.F., Kwong, E.M.L., Tang, A.H.N., Ng, I.O.L., et al. (2021). Suppression of ACADM-Mediated Fatty Acid Oxidation Promotes Hepatocellular Carcinoma via Aberrant CAV1/SREBP1 Signaling. Cancer Res. *81*, 3679–3692. https://doi.org/10.1158/0008-5472.CAN-20-3944.
47. Vila, I.K., Chamma, H., Steer, A., Saccas, M., Taffoni, C., Turtoi, E., Reinert, L.S., Hussain, S., Marines, J., Jin, L., et al. (2022). STING orchestrates the crosstalk between polyunsaturated fatty acid metabolism and inflammatory responses. Cell Metab. *34*, 125–139. https://doi.org/10.1016/j.cmet.2021.12.007.
48. Du, X., Chapman, N.M., and Chi, H. (2018). Emerging Roles of Cellular Metabolism in Regulating Dendritic Cell Subsets and Function. Front. Cell Dev. Biol. *6*, 152. https://doi.org/10.3389/fcell.2018.00152.
49. Herber, D.L., Cao, W., Nefedova, Y., Novitskiy, S.V., Nagaraj, S., Tyurin, V. A., Corzo, A., Cho, H.I., Celis, E., Lennox, B., et al. (2010). Lipid accumulation and dendritic cell dysfunction in cancer. Nat. Med. *16*, 880–886. https://doi.org/10.1038/nm.2172.
50. Huang, X., Yi, S., Hu, J., Du, Z., Wang, Q., Ye, Z., Su, G., Kijlstra, A., and Yang, P. (2021). Linoleic acid inhibits in vitro function of human and murine

dendritic cells, CD4(+)T cells and retinal pigment epithelial cells. Graefes Arch. Clin. Exp. Ophthalmol. *259*, 987–998. https://doi.org/10.1007/s00417-020-04972-6.

51. Cloherty, A.P.M., Olmstead, A.D., Ribeiro, C.M.S., and Jean, F. (2020). Hijacking of Lipid Droplets by Hepatitis C, Dengue and Zika Viruses-From Viral Protein Moonlighting to Extracellular Release. Int. J. Mol. Sci. *21*, 7901. https://doi.org/10.3390/ijms21217901.

52. Read, S.A., Tay, E., Shahidi, M., George, J., and Douglas, M.W. (2014). Hepatitis C virus infection mediates cholesteryl ester synthesis to facilitate infectious particle production. J. Gen. Virol. *95*, 1900–1910. https://doi.org/10.1099/vir.0.065300-0.

53. Liefhebber, J.M.P., Hague, C.V., Zhang, Q., Wakelam, M.J.O., and McLauchlan, J. (2014). Modulation of triglyceride and cholesterol ester synthesis impairs assembly of infectious hepatitis C virus. J. Biol. Chem. *289*, 21276–21288. https://doi.org/10.1074/jbc.M114.582999.

54. Schmidt, N.M., Wing, P.A.C., Diniz, M.O., Pallett, L.J., Swadling, L., Harris, J.M., Burton, A.R., Jeffery-Smith, A., Zakeri, N., Amin, O.E., et al. (2021). Targeting human Acyl-CoA:cholesterol acyltransferase as a dual viral and T cell metabolic checkpoint. Nat. Commun. *12*, 2814. https://doi.org/10.1038/s41467-021-22967-7.

55. Hu, L., Li, J., Cai, H., Yao, W., Xiao, J., Li, Y.P., Qiu, X., Xia, H., and Peng, T. (2017). Avasimibe: A novel hepatitis C virus inhibitor that targets the assembly of infectious viral particles. Antiviral. Res. *148*, 5–14. https://doi.org/10.1016/j.antiviral.2017.10.016.

56. (2024). In Brief: RSV vaccine (Arexvy) for ages 50-59. Med. Lett. Drugs Ther. *66*, 113–114. https://doi.org/10.58347/tml.2024.1707a.

57. Dias, S.S.G., Soares, V.C., Ferreira, A.C., Sacramento, C.Q., Fintelman-Rodrigues, N., Temerozo, J.R., Teixeira, L., Nunes da Silva, M.A., Barreto, E., Mattos, M., et al. (2020). Lipid droplets fuel SARS-CoV-2 replication and production of inflammatory mediators. PLoS Pathog. *16*, e1009127. https://doi.org/10.1371/journal.ppat.1009127.

58. Namazue, J., Kato, T., Okuno, T., Shiraki, K., and Yamanishi, K. (1989). Evidence for attachment of fatty acid to varicella-zoster virus glycoproteins and effect of cerulenin on the maturation of varicella-zoster virus glycoproteins. Intervirology *30*, 268–277. https://doi.org/10.1159/000150102.

59. Li, Y., Webster-Cyriaque, J., Tomlinson, C.C., Yohe, M., and Kenney, S. (2004). Fatty acid synthase expression is induced by the Epstein-Barr virus immediate-early protein BRLF1 and is required for lytic viral gene expression. J. Virol. *78*, 4197–4206. https://doi.org/10.1128/jvi.78.8.4197-4206.2004.

60. Qiu, C.C., Atencio, A.E., and Gallucci, S. (2019). Inhibition of fatty acid metabolism by etomoxir or TOFA suppresses murine dendritic cell activation without affecting viability. Immunopharmacol. Immunotoxicol. *41*, 361–369. https://doi.org/10.1080/08923973.2019.1616754.

61. Nguyen-Phuong, T., Chung, H., Jang, J., Kim, J.S., and Park, C.G. (2022). Acetyl-CoA carboxylase-1/2 blockade locks dendritic cells in the semimature state associated with FA deprivation by favoring FAO. J. Leukoc. Biol. *111*, 539–551. https://doi.org/10.1002/JLB.1A0920-561RR.

62. Chen, X., Song, Q., Xia, L., and Xu, X. (2017). Synergy of Dendritic Cell Vaccines and Avasimibe in Treatment of Head and Neck Cancer in Mice. Med. Sci. Monit. *23*, 4471–4476. https://doi.org/10.12659/msm.905814.

63. Ma, S., Lv, M., Chen, X., Zang, G., Tang, Z., Zhang, Y., and Hu, W. (2023). Avasimibe can cooperate with a DC-targeting and integration-deficient lentivector to induce stronger HBV specific T cytotoxic response by regulating cholesterol metabolism. Antivir. Res. *216*, 105662. https://doi.org/10.1016/j.antiviral.2023.105662.

64. Yang, W., Bai, Y., Xiong, Y., Zhang, J., Chen, S., Zheng, X., Meng, X., Li, L., Wang, J., Xu, C., et al. (2016). Potentiating the antitumour response of CD8(+) T cells by modulating cholesterol metabolism. Nature *531*, 651–655. https://doi.org/10.1038/nature17412.

65. Xia, Y., Xie, Y., Yu, Z., Xiao, H., Jiang, G., Zhou, X., Yang, Y., Li, X., Zhao, M., Li, L., et al. (2018). The Mevalonate Pathway Is a Druggable Target for Vaccine Adjuvant Discovery. Cell *175*, 1059–1073. https://doi.org/10.1016/j.cell.2018.08.070.

66. Blankenberg, D., Von Kuster, G., Coraor, N., Ananda, G., Lazarus, R., Mangan, M., Nekrutenko, A., and Taylor, J. (2010). Galaxy: a web-based genome analysis tool for experimentalists. Curr. Protoc. Mol. Biol. *19*, 19.10.1–19.10.21. https://doi.org/10.1002/0471142727.mb1910s89.

67. Pratt, D., Chen, J., Welker, D., Rivas, R., Pillich, R., Rynkov, V., Ono, K., Miello, C., Hicks, L., Szalma, S., et al. (2015). NDEx, the Network Data Exchange. Cell Syst. *1*, 302–305. https://doi.org/10.1016/j.cels.2015.10.001.

68. Subramanian, A., Tamayo, P., Mootha, V.K., Mukherjee, S., Ebert, B.L., Gillette, M.A., Paulovich, A., Pomeroy, S.L., Golub, T.R., Lander, E.S., and Mesirov, J.P. (2005). Gene set enrichment analysis: a knowledge-based approach for interpreting genome-wide expression profiles. Proc. Natl. Acad. Sci. USA *102*, 15545–15550. https://doi.org/10.1073/pnas.0506580102.

69. Schindelin, J., Arganda-Carreras, I., Frise, E., Kaynig, V., Longair, M., Pietzsch, T., Preibisch, S., Rueden, C., Saalfeld, S., Schmid, B., et al. (2012). Fiji: an open-source platform for biological-image analysis. Nat. Methods *9*, 676–682. https://doi.org/10.1038/nmeth.2019.

70. Xia, J., Psychogios, N., Young, N., and Wishart, D.S. (2009). MetaboAnalyst: a web server for metabolomic data analysis and interpretation. Nucleic Acids Res. *37*, W652–W660. https://doi.org/10.1093/nar/gkp356.

71. Pietzke, M., and Vazquez, A. (2020). Metabolite AutoPlotter - an application to process and visualise metabolite data in the web browser. Cancer Metabol. *8*, 15. https://doi.org/10.1186/s40170-020-00220-x.

72. Karnovsky, A., Weymouth, T., Hull, T., Tarcea, V.G., Scardoni, G., Laudanna, C., Sartor, M.A., Stringer, K.A., Jagadish, H.V., Burant, C., et al. (2012). Metscape 2 bioinformatics tool for the analysis and visualization of metabolomics and gene expression data. Bioinformatics *28*, 373–380. https://doi.org/10.1093/bioinformatics/btr661.

73. Shannon, P., Markiel, A., Ozier, O., Baliga, N.S., Wang, J.T., Ramage, D., Amin, N., Schwikowski, B., and Ideker, T. (2003). Cytoscape: a software environment for integrated models of biomolecular interaction networks. Genome Res. *13*, 2498–2504. https://doi.org/10.1101/gr.1239303.

74. Collins, N., Jiang, X., Zaid, A., Macleod, B.L., Li, J., Park, C.O., Haque, A., Bedoui, S., Heath, W.R., Mueller, S.N., et al. (2016). Skin CD4(+) memory T cells exhibit combined cluster-mediated retention and equilibration with the circulation. Nat. Commun. *7*, 11514. https://doi.org/10.1038/ncomms11514.

75. Gonzalez, P.A., Prado, C.E., Leiva, E.D., Carreno, L.J., Bueno, S.M., Riedel, C.A., and Kalergis, A.M. (2008). Respiratory syncytial virus impairs T cell activation by preventing synapse assembly with dendritic cells. Proc. Natl. Acad. Sci. USA *105*, 14999–15004. https://doi.org/10.1073/pnas.0802555105.

76. Matyash, V., Liebisch, G., Kurzchalia, T.V., Shevchenko, A., and Schwudke, D. (2008). Lipid extraction by methyl-tert-butyl ether for high-throughput lipidomics. J. Lipid Res. *49*, 1137–1146. https://doi.org/10.1194/jlr.D700041-JLR200.

77. Cajka, T., and Fiehn, O. (2016). Increasing lipidomic coverage by selecting optimal mobile-phase modifiers in LC-MS of blood plasma. Meta *12*, ARTN 34. https://doi.org/10.1007/s11306-015-0929-x.

78. Cajka, T., and Fiehn, O. (2016). Increasing lipidomic coverage by selecting optimal mobile-phase modifiers in LC–MS of blood plasma. Metabolomics *12*, 1–11.

79. Tsugawa, H., Ikeda, K., Takahashi, M., Satoh, A., Mori, Y., Uchino, H., Okahashi, N., Yamada, Y., Tada, I., Bonini, P., et al. (2020). A lipidome atlas in MS-DIAL 4. Nat. Biotechnol. *38*, 1159–1163. https://doi.org/10.1038/s41587-020-0531-2.

80. Sumner, L.W., Amberg, A., Barrett, D., Beale, M.H., Beger, R., Daykin, C.A., Fan, T.W.M., Fiehn, O., Goodacre, R., Griffin, J.L., et al. (2007). Proposed minimum reporting standards for chemical analysis Chemical Analysis Working Group (CAWG) Metabolomics Standards Initiative (MSI). Metabolomics *3*, 211–221. https://doi.org/10.1007/s11306-007-0082-2.

81. Alseekh, S., Aharoni, A., Brotman, Y., Contrepois, K., D'Auria, J., Ewald, J., C Ewald, J., Fraser, P.D., Giavalisco, P., Hall, R.D., et al. (2021). Mass spectrometry-based metabolomics: a guide for annotation, quantification and best reporting practices. Nat. Methods *18*, 747–756. https://doi.org/10.1038/s41592-021-01197-1.

82. Kind, T., Liu, K.H., Lee, D.Y., DeFelice, B., Meissen, J.K., and Fiehn, O. (2013). LipidBlast in silico tandem mass spectrometry database for lipid identification. Nat. Methods *10*, 755–758. https://doi.org/10.1038/nmeth.2551.

83. Fahy, E., Sud, M., Cotter, D., and Subramaniam, S. (2007). LIPID MAPS online tools for lipid research. Nucleic Acids Res. *35*, W606–W612. https://doi.org/10.1093/nar/gkm324.

84. Aimo, L., Liechti, R., Hyka-Nouspikel, N., Niknejad, A., Gleizes, A., Götz, L., Kuznetsov, D., David, F.P.A., van der Goot, F.G., Riezman, H., et al. (2015). The SwissLipids knowledgebase for lipid biology. Bioinformatics *31*, 2860–2866. https://doi.org/10.1093/bioinformatics/btv285.

85. Duhrkop, K., Fleischauer, M., Ludwig, M., Aksenov, A.A., Melnik, A.V., Meusel, M., Dorrestein, P.C., Rousu, J., and Bocker, S. (2019). SIRIUS 4: a rapid tool for turning tandem mass spectra into metabolite structure information. Nat. Methods *16*, 299–302. https://doi.org/10.1038/s41592-019-0344-8.

86. Wang, F., Allen, D., Tian, S., Oler, E., Gautam, V., Greiner, R., Metz, T.O., and Wishart, D.S. (2022). CFM-ID 4.0 - a web server for accurate MS-based metabolite identification. Nucleic Acids Res. *50*, W165–W174. https://doi.org/10.1093/nar/gkac383.

87. Wishart, D.S., Guo, A., Oler, E., Wang, F., Anjum, A., Peters, H., Dizon, R., Sayeeda, Z., Tian, S., Lee, B.L., et al. (2022). HMDB 5.0: the Human Metabolome Database for 2022. Nucleic Acids Res. *50*, D622–D631. https://doi.org/10.1093/nar/gkab1062.

88. Liebisch, G., Vizcaíno, J.A., Köfeler, H., Trötzmüller, M., Griffiths, W.J., Schmitz, G., Spener, F., and Wakelam, M.J.O. (2013). Shorthand notation for lipid structures derived from mass spectrometry. J. Lipid Res. *54*, 1523–1530. https://doi.org/10.1194/jlr.M033506.

89. Pauling, J.K., Hermansson, M., Hartler, J., Christiansen, K., Gallego, S.F., Peng, B., Ahrends, R., and Ejsing, C.S. (2017). Proposal for a common nomenclature for fragment ions in mass spectra of lipids. PLoS One *12*, e0188394. https://doi.org/10.1371/journal.pone.0188394.

STAR★METHODS

KEY RESOURCES TABLE

REAGENT or RESOURCE	SOURCE	IDENTIFIER
Antibodies		
Mouse PERCP anti-CD11c clone N418	BioLegend	Cat#117326; RIDD: AB_2129643
Mouse anti-gD Ab Clone 2C10	Virusys	Cat#HA025-1; RIDD: AB_2713937; Lot #F1856157
Mouse anti-gB Ab Clone 10B7	Virusys	Cat#HA056-1; RIDD: AB_2713936; Lot #H1755112
Mouse anti-VP16 Ab Clone 1-21	Santa Cruz Biotechnology	Cat#sc-7545; RIDD: AB_628443; Lot #G1709
Mouse HRP-anti-β-actin mAb Clone 2D1D10	GenScript	Cat#A00730; RIDD: AB_914100; Lot #16C0011012
Goat anti-mouse IgG (H+L)-HRP conjugate secondary	BioRad	Cat#1706516; Lot #64434263
Anti-rabbit IgG Horseradish Peroxidase linked F(ab')s fragment	GE Healthcare UK Limited	Cat#NA9340V; Lot#9653376
Mouse PE anti-I-Ab Ab Clone AF6-88.5	BioLegend	Cat#116508; RIDD: AB_313735; Lot #B354788
Mouse APC anti-H-2Kb Ab Clone AF6-120.1	BioLegend	Cat#116418; RIDD: AB_10574160; Lot #B366826
Mouse APC anti-CD40 Ab Clone 3/23	BioLegend	Cat#124612; RIDD: AB_1134072; Lot #B351628
Mouse PE anti-CD80 Ab Clone 16-10A1	BioLegend	Cat#104707; RRID: AB_313128; Lot #B340153
Mouse PE anti-CD83 Ab Clone Michel-19	BioLegend	Cat#121507; RRID: AB_572014; Lot #B215191
Mouse APC anti-CD86 Ab Clone GL-1	BioLegend	Cat#105012; RRID: AB_493342; Lot #B346110
Mouse PE anti-CD103 Ab Clone 2E7	BioLegend	Cat#121406; RRID: AB_1133989; Lot #B353762
Mouse APC anti-CD207 Ab Clone 4C7	BioLegend	Cat#144205; RRID: AB_2561997; Lot #B191420
Mouse FITC anti-CD4 Ab Clone RM4-4	BioLegend	Cat#116004; RRID: AB_313689; Lot #B172845
Mouse AlexaFluor 700 anti-CD4 Ab Clone GK1.5	eBioscience	Cat#56-0041-82; Lot #E025940
Mouse PE anti-CD8a Clone Ly-2	PharMingen	Cat#553033; Lot #27653
Mouse FITC anti-CD8 Ab Clone 53-6.7	BioLegend	Cat#100706; RRID: AB_312745; Lot #B195504
Mouse PERCP anti-CD25 Ab Clone PC61	BioLegend	Cat#102028; RRID: AB_2295974; Lot #B353747
Mouse APC anti-CD71 Ab Clone RI7217	BioLegend	Cat#113820; RRDI: AB_2728135; Lot #B364530
Rat Anti-mouse IL-2 Ab Clone JES6-1A12	BD Bioscience	Cat#554424; RRID: AB_395383; Lot #8314561
Biotin anti-mouse IL-2 Clone JES6-5H4	BioLegend	Cat#503804; RRID: AB_315298; Lot #B187183
Mouse anti-IL-4 Ab Clone 11B11	BioLegend	Cat#504102; RRID: AB_315316; Lot #B344376
Biotin anti-mouse IL-4 Ab Clone BVD6-24G2	BioLegend	Cat#504202; RRID: AB_315324; Lot #B336288
Rat anti-mouse IFN-γ Ab Clone AN-18	BD Bioscience	Cat#551309; RRID: AB_394145; Lot #9052716
Biotin Rat anti-mouse IFN-γ Ab Clone XMG1.2	BD Bioscience	Cat#554410; RRID: AB_395374; Lot #9081615
FATP2	Cell Signaling	Cat#78771T
DGAT2	Santa Cruz Biotechnology	Cat#sc-293211; RRID: AB_3674369
CD36 (SMϕ)	Santa Cruz Biotechnology	Cat#sc-7309; RRID: AB_627044
Bacterial and virus strains		
HSV-1 strain F	ATCC	VR-733
HSV-1 strain KOS	ATCC	VR-1493
HSV-1 strain 17syn$^+$	Kindly provided by Dr Carola Otth, Universidad Austral de Chile, Chile	N/A
Biological samples		
Primary bone marrow-derived cells from C57BL/6 WT mice	The Jackson Laboratory	N/A
Primary CD4$^+$ T cells from C57BL/6 gDT-II mice	Dr. Francis Carbone Laboratory	N/A
Primary CD8$^+$ T cells from C57BL/6 gBT-I mice	Dr. Francis Carbone Laboratory	N/A

(*Continued on next page*)

Continued

REAGENT or RESOURCE	SOURCE	IDENTIFIER
Chemicals, peptides, and recombinant proteins		
Lipofermata	Cayman Chemical	Cat#25869; CAS No. 297180-15-5
Sulfosuccinimidyl oleate	Cayman Chemical	Cat#11211; CAS No. 1212012-37-7
5-(tetradecycloxy)-2-furancarboxylic acid (TOFA)	Cayman Chemical	Cat#10005263; CAS No. 54857-86-2
Triacsin C	Cayman Chemical	Cat#10007448; CAS No. 76896-80-5
A922500	Cayman Chemical	Cat#10012708; CAS No. 959122-11-3
PF-06424439	Cayman Chemical	Cat#17680; CAS No. 1469284-79-4
Avasimibe	Cayman Chemical	Cat#18129; CAS No. 166518-60-1
CAY10499	Cayman Chemical	Cat#10007875; CAS No. 359714-55-9
BODIPY 493/503	Cayman Chemical	Cat#25892; CAS No. 121207-31-6
LipidTOX Red	Thermo Fisher Scientific	Cat#H34476
BODIPY-FL-C16	Thermo Fisher Scientific	Cat#D3821
Critical commercial assays		
TaqMan Array Mouse Lipid Regulated Genes	Applied Biosystems	Cat#4418846
Proteome Profile Mouse XL Cytokine Array	R&D SYSTEMS	Cat#ARY028
Deposited data		
RNA-seq	This paper; Gene Expression Omnibus database (GEO)	GSE238169; URL: https://www.ncbi.nlm.nih.gov/geo/query/acc.cgi?acc=GSE238169.
Lipidomic data	This paper, Metabolights	MTBLS5163; URL: https://www.ebi.ac.uk/metabolights/editor/MTBLS5163/descriptors.
Experimental models: Cell lines		
Vero Cells	ATCC	CCL-81
Experimental models: Organisms/strains		
C57BL/6J mice	The Jackson Laboratory	Strain #:000664; RRID:IMSR_JAX:000664
gBT-I mice	Dr. Francis Carbone Laboratory	N/A
gDT-II mice	Dr. Francis Carbone Laboratory	N/A
Oligonucleotides		
Dgat1 (Mm00515643_m1)	Life Technologies	Cat#4453320
Dgat2 (Mm00499530_m1)	Life Technologies	Cat#4448892
Slc27a2 (Mm00449517_m1)	Life Technologies	Cat#4448892
Soat1 (Mm00486279_m1)	Life Technologies	Cat#4448892
Plin3 (Mm04208646_g1)	Life Technologies	Cat#4453320
Pnpla2 (Mm00503040_m1)	Life Technologies	Cat#4453320
Gapdh (Mm99999915_g1)	Life Technologies	Cat#4453320
Acaca (Mm01304289_m1)	Life Technologies	Cat#4448892
Acsl1 (Mm00484217_m1)	Life Technologies	Cat#4448892
Software and algorithms		
Ingenuity pathway analysis (IPA)	Qiagen	Qiagen version #84978992. https://digitalinsights.qiagen.com/products-overview/discovery-insights-portfolio/analysis-and-visualization/qiagen-ipa/
Galaxy	Blankenberg et al.[66]	usegalaxy.org
NDEX WebApp	Pratt et al.[67]	https://www.ndexbio.org/index.html#/network/5c9c2021-bcdb-11ef-99aa-005056ae3c32

(*Continued on next page*)

Continued

REAGENT or RESOURCE	SOURCE	IDENTIFIER
GSEA	Subramanian et al.[68]	GSEA software (version 4.3.2) (https://www.gsea-msigdb.org/gsea/index.jsp).
FlowJo 10 software	BD Bioscience	https://www.flowjo.com/solutions/flowjo/downloads
Leica Application Suite X (LAS X)	Leica Microsystems	https://www.leica-microsystems.com/es/productos/software-de-microscopia/p/leica-las-x-ls/downloads/
Fiji Image J	Schindelin et al.[69]	https://imagej.net/software/fiji/#license
Reifycs ABFconverter software		https://www.reifycs.com/abfconverter/
Metaboanalyst 5.0	Xia et al.[70]	https://www.metaboanalyst.ca/
Metabolite AutoPlotter v2.6	Pietzke et al.[71]	https://mpietzke.shinyapps.io/autoplotter
MetScape v3.1.3	Karnovsky et al.[72]	https://metscape.ncibi.org/
Cytoscape v3.9.1	Shannon et al.[73]	https://cytoscape.org/index.html
Compass DataAnalysis 4.4.200 (Bruker) software		https://www.bruker.com/en/products-and-solutions/mass-spectrometry/ms-software.html
GraphPad Prism 9 (GraphPad Software).	GraphPad Prism (RRID:SCR_002798)	https://www.graphpad.com/

EXPERIMENTAL MODEL AND STUDY PARTICIPANT DETAILS

Mice

C57BL/6J female and male mice were originally sourced from The Jackson Laboratory (Bar Harbor, ME). 6 to 8-week-old female and male gBT-I and gDT-II transgenic mice, encoding HSV-specific T cell receptors that recognize H-2Kb (MHC-I)/$gB_{498\text{-}505}$ and I-Ab (MHC-II)/$gD_{290\text{-}302}$, respectively were shared by Dr. Francis Carbone.[35,74] Male and female animals were Indistinguishably used for *in vivo* experiments. All mice were housed at the central animal facility of the Pontificia Universidad Católica de Chile and handled according to the guidelines of the Institutional Scientific Ethics Committee for Animal Care and the Environment. This study was approved under Protocol n° CEC190902006.

Virus

HSV-1 strain F (ATCC VR-733), strain KOS (ATCC VR-1493) and strain $17syn^+$, provided by Dr. Carola Otth (Universidad Austral de Chile, Chile) were propagated in Vero cells (ATCC CCL-81). Briefly, T175 flasks with Vero cells monolayers were inoculated with $2x10^5$ plaque forming units (PFU) of HSV-1 (multiplicity of infection, MOI of 0.01) in 13 ml of Opti-MEM (Gibco, Life Technologies, cat Nº 22600-043) supplemented with 100 U/ml penicillin-streptomycin (100x stock, Thermo Fisher Scientific, #cat 15140122) and incubated at 37°C for 48 h until visible cytopathic effect. Then, the content of the flasks was pooled and sonicated in an ultrasonic bath for 10 min with pulses of 15 seconds. Then, the cell debris was centrifugated at 6,500 revolutions per minute (rpm) for 10 min. The supernatants were stored at -80°C until use. HSV-1 strains were tittered over Vero cells in flat-bottom 96-wells plates and screened for plaque production under a ZEISS Axio Vert.1A inverted microscope.

Cell lines

Vero cells (ATCC CCL-81) were cultured in DMEM (Thermo Fisher Scientific, cat#12100-038) supplemented with 10% FBS (Biowest, cat#S1810), 1 mM non-essential amino acids (Thermo Fisher Scientific, cat#11140050), and 100 U/ml penicillin-streptomycin (100x stock, Thermo Fisher Scientific, cat#15140122). Cells were passaged every 3-5 days by dilution of 1:5 to 1:10, after releasing the attached cells using Trypsin (Thermo Fisher Scientific cat#15090046). Cells utilized for virus production were not authenticated after acquisition. Mycoplasma components were not detected in cell preparations utilized for virus expansion.

Primary cell cultures

Bone marrow derived dendritic cells (BMDCs) were differentiated from hind limb bone marrow precursors of C57BL/6J female or male mice indistinguishably, in Roswell Park Memorial Institute-1640 (RPMI-1640) media (Cytiva, cat#SH30255.FS) supplemented with 10% fetal bovine serum (Biowest, cat#S1810), 100 UI/ml Penicillin/Streptomycin, and 10 ng/ml of recombinant murine granulocyte-macrophage-colony-stimulating factor (GM-CSF, GenScript cat#Z03300), as previously described.[75] The culture media was replaced every 48 h after 6 days of culture. BMDCs were authenticated by flow cytometry using the CD11c marker. Mycoplasma was not tested in these cells, as they were directly derived from bone marrow progenitors as a primary culture.

METHOD DETAILS

DC infection with HSV-1

Bone marrow-derived dendritic cells (BMDCs) were differentiated from hind limb bone marrow precursors of C57BL/6J mice as previously described.[75] After six days of culture, BMDCs were infected with HSV-1 strains F, KOS, or 17syn$^+$ at a multiplicity of infection (MOI) of 3 for 1 h at 37°C, then washed with culture media and collected and analysed for infection and viability at 12- and 18-hours post-infection (hpi).

Pharmacological treatment of DCs

BMDCs were treated for 3 h with inhibitors and then infected with HSV-1 strain F MOI 3 for 1 h. Then, DCs were treated for 11 or 17 h with the inhibitors and different cellular analyses were performed. The lipid metabolism inhibitors (all from Cayman chemical) were lipofermata-10 μM (FATP inhibitor), sulfosuccinimidyl oleate-50 μM (SSO-CD36 inhibitor), 5-(tetradecycloxy)-2-furancarboxylic acid (TOFA)-10 μM (ACC inhibitor), Triacsin C-10 μM (ACS inhibitor), A922500-10 μM (DGAT1 inhibitor), PF-06424439-10 μM (DGAT2 inhibitor), Avasimibe-10 μM (ACAT1 and ACAT2 inhibitor) and CAY10499-10 μM (Lipase inhibitor).

Lipid metabolism-related gene expression by RT-qPCR

RNA was isolated from HSV-1 strain F-infected BMDCs 12 hpi using TRIzol (Thermo Fisher Scientific) and retrotranscribed to cDNA using SuperScriptTM II reverse transcriptase (Invitrogen). qPCR reactions were carried out using TaqMan Master Mix, TaqMan array mouse lipid regulated genes (cat#4418846) and TaqMan probes for *Dgat1*, *Dgat2*, *Slc27a2*, *Soat1*, *Plin3*, *Pnpla2*, and *Gapdh* in a StepOnePlusTM Real-time PCR System (Applied Biosystems). The abundance of each target mRNA was determined by relative expression to the *gapdh* housekeeping gene using the $2^{-(\Delta\Delta Ct)}$ method.

Ingenuity pathway analysis (IPA)-RT-qPCR

RT-qPCR data was imported into the Qlucore Omics Explorer software (version 3.8, Qlucore) and transformed into $\log_2$ values. A t-test student was performed over the remaining data and the results were exported containing the $\log_2$ ratio and UniProt identifier code for each mRNA expression. The dataset was uploaded to Ingenuity Pathway Analysis (IPA) (version 84978992, Qiagen), where relevant networks were identified through the Core Analysis feature, considering a p-value <0.05. Those genes displaying significant changes were listed and then added and represented as nodes to build a custom network. Nodes were related to each other considering either indirect or direct interactions through the ''Connect'' tool. The activity processes of each node were simulated and overlaid onto the network considering downstream and upstream effects and the $\log_2$ ratios found in the Core Analysis previously performed, using the ''Molecule Activity Predictor'' (MAP) tool.

Transcriptomic analyses of lipid metabolism-related genes

HSV-1 strain F-infected or MOCK treated BMDCs for 12 hours were washed thrice with PBS and resuspended in TRIzol (Thermo Fisher Scientific) for RNA purification. RNA integrity was evaluated by Bioanalyzer 2100 (Agilent), and qualified samples were processed for library construction. cDNA library construction was performed with TruSeq stranded mRNA kit (Illumina) and quantified by qPCR. Illumina sequencing was performed at Genoma Mayor, Universidad Mayor, Chile. RNA-seq data analysis was performed using the webserver Galaxy (usegalaxy.org). The workflow included the Trim Galore tool to delete Illumina universal adapters and the Trimmomatic tool to cut bad-quality sequences. Alignment processes were performed by HISAT2 using the mm10 genome. Reads were counted with the HT-count tool, and differential expression analysis was performed with the Deseq2 tool. The RNA-seq network analysis was deposited into the NDEx WebApp at the following URL: https://www.ndexbio.org/#/network/5c9c2021-bcdb-11ef-99aa-005056ae3c32. RNA-seq data were deposited in the Gene Expression Omnibus database (GEO) under accession number GSE238169 and BioProject accession number PRJNA998087 available at the following URL: https://www.ncbi.nlm.nih.gov/geo/query/acc.cgi?acc=GSE238169.

TNF-α cytokine detection

BMDCs were purified with a Pan Dendritic Cell Isolation Kit (Miltenyi Biotec, Cat#130-100-875) and then infected with HSV-1 strain F MOI 3 or inoculated with MOCK preparations for 18 h. After this period, the supernatant was recovered to measure TNF-α. For this, the supernatant of BMDCs was incubated in the Mouse XL Cytokine Array (R&D SYSTEMS, cat#ARY028), according to the manufacturer's instructions. The levels of cytokines were quantified by densitometry using ImageJ.

Neutral lipid measurements

HSV-1-infected BMDCs at 12 and 18 hpi were stained with a neutral lipid probe (HCS LipidTOX^{TM} Red (Thermo Fisher Scientific)) the viability marker Zombie NIR (BioLegend) and the DC marker anti-CD11c clone N418 antibody (BioLegend) for 30 minutes and washed twice with PBS. Then, DCs were fixed with 2% paraformaldehyde (PFA) for 30 minutes, washed with PBS, and resuspended in PBS for flow cytometry analyses using FACSCANTO II and FACSVia cytometers (BD Biosciences). Cytometry analyses were performed using FlowJo 10 software (BD Biosciences) (see Figure S7A).

Confocal microscopy

BMDCs were infected with HSV-1 strain F, KOS, or 17syn$^+$ for 12 or 18 h, washed with PBS and stained for 15 minutes with a neutral lipids probe (BODIPY 493/503 5 mM, Cayman) and DAPI (Tocris). DCs were fixed with 4% PFA for 30 minutes, washed with PBS 1X, and mounted using Prolong (Thermo Fisher Scientific) for analysis by Leica SP8 confocal microscopy at 100x. Images were processed using Leica Application Suite X (LAS X) software and analysed with Fiji software to measure the amount and size of BODIPY493/503 neutral lipid structures.

Transmission electron microscopy

HSV-1 strain F-infected BMDCs for 12 and 18 h were fixed with 2.5% glutaraldehyde in cacodylate buffer and processed at the Advanced Microscopy Unit (UMA) of the Faculty of Biological Sciences at the Pontificia Universidad Católica de Chile. Transmission electron microscopy (TEM) images were obtained using a Philips Tecnai 12 microscopy (Biotwin) and the iTEM Olympus Soft Imaging Solution software (Windows NT 6.1) at 4200x magnification. Fiji software was used to measure the number and size of LDs.

Lipid uptake assay

BMDCs were treated for 3 hours with lipofermata-10 μM or SSO-50 μM. Palmitic acid (100 μM, Cayman Chemical) conjugated to fatty acid-free bovine serum albumin (Sigma-Aldrich) was used as fatty acid uptake control. Then, DCs were infected with HSV-1 strain F MOI 3.0 for 1 h for adsorption and returned to treatment with the FATP and CD36 inhibitors and BODIPY-FL-C16 probe 1:2,500 (Thermo Fisher Scientific). After 11 hours, DCs were washed with PBS 1X to eliminate excess probe, stained with Zombie NIR viability marker (BioLegend) and anti-CD11c clone N418 antibody (BioLegend), and fixed with PFA 2% for 30 minutes. Samples were acquired in a FACSCANTO II cytometer (BD Biosciences), and the data were analysed using the FlowJo 10 software (BD Biosciences).

Ultra-high performance liquid chromatography-quadrupole time-of-flight (UHPLC-QTOF) analysis

BMDCs were infected with HSV-1 strain F MOI 3 for 12 or 18h, then washed thrice with H_2O hypergrade (Merck), resuspended, and scraped in cold methanol hypergrade (Merck). Samples were dried using a CentriVap (Labconco) and lyophilized, followed by Matyash extraction with minor modifications.[76] Dried samples were extracted with 50 μl water, 150 μl methanol and 500 μl methyl tert-butyl ether (MTBE), homogenized at 2,000 rpm using a Thermomixer C (Eppendorf) for 7 min at 4°C, then 250 μl water was added to separate aqueous and organic phases. Samples were homogenized for 3 min and centrifuged for 12 min at 13,000 g to recover 300 μl of the organic phase in a Heraeus-Fresco17 centrifuge (Thermo Fisher Scientific). The lipid phase was dried and resuspended in 300 μl of methanol/isopropanol (1:1) and homogenized for 5 min before UHPLC-QTOF analysis, following Cajka et al., 2016 recommendations.[77] Extraction blanks and pooled samples were used as quality control (QC) of analytical variation and was obtained by mixing 50 μl of each resuspended sample. Results were normalized using total proteins left in the extracted samples by Bradford protein assay with a Synergy HTX multi-mode reader. The lipidomic analysis was carried out with a UHPLC Bruker Elute LC system coupled in tandem with a Q-TOF spectrometer Compact, Bruker (Bremen, Germany). The control system was Compass HyStar (Bruker), and the acquisition software was Bruker oTOF control v4.1.402.322-7977-vc110 6.3.3.11. The lipid extracts were analysed using the UHPLC method.[78] Lipids were separated using a Kinetex® C18 column (100 x 4.6mm; 2.6 μm, Phenomenex) coupled to a SecurityGuard^{TM} ULTRA C18 precolumn (Phenomenex) maintained at 65°C and at a flow rate of 0.6 ml/min. Mobile phase A consisted in 60:39.9:0.1 (%v/v/v) acetonitrile: water: formic acid with 10 mM ammonium formate, and mobile phase B consisted in 90:9.9:0.1 (%v/v/v) isopropanol: acetonitrile: formic acid with 10 mM ammonium formate. Reconstituted lipid extract (20 μl) was injected into the system in partial loop mode, and the total run was 25 min. All solvents and modifiers were liquid chromatography-mass spectrometry (LC-MS) grade. The MS conditions were positive ionization ESI +4500 V; dry gas, 9 l/min; nebulizer, 4 Bar; 200°C; end capillary 500 V; collision energy at 10–25 eV in stepping mode; Auto MS/MS mode (2 precursor/cycle), 50–1,500 m/z (scan 0.2 s centroid mode); and internal calibration using sodium formate (0.01 M) with a mass accuracy < 3 ppm. All metabolomic sequences started with 5 blank injections (resuspension solvent only), followed by 3 technical blanks (considering the extraction process) and 3 QC. Then, for every 11 samples, a QC was injected.

Data processing

Raw Bruker data was transformed as ABF format using Reifycs ABFconverter software. Then, peak table and lipid annotation was elaborated using MS-DIAL 4 software[79] under the following parameters: MS1 and MS2 tolerance: 0.02 and 0.05 Da, retention time (Rt) begin-end: 0.5 - 14 min. MS1 and MS/MS begin-end: 50–1,500 Da. Minimum peak height: 500 amplitude, Mass slice width: 0.05 Da. MS2 Dec and MS/MS abundance cut off at default settings. MS-DIAL LipidBlast was used as an MSP file, and identification settings as default. Adduct included were $[M+H]^+$, $[M+NH_4+]$, $[M+Na]^+$, $[M+ACN+H]^+$, $[2M+H]^+$, $[2M+NH_4]^+$ and $[2M+Na]^+$. The reference alignment file was QC samples, with Rt tolerance: 0.2 min, MS1 tolerance: 0.03 Da, Rt factor: 0.5, MS1 factor: 0.5, Peak count filter: 0% and N% detected in at least one group: 0%. To compensate Rt shift, QC LOESS (Locally Weighted Scatter-plot Smoothing) alignment was performed prior matrix export. This software transformed the raw data into a .txt data matrix which includes several features (peak number, m/z, Rt, annotation, lipid class, isotopes, MS/MS spectra and normalized peak intensity). Then, QC LOESS normalized peak intensity was normalized by protein concentration from each sample, and the average value was used in the QC samples since these QC were equal aliquots from each analysed sample.

Data prefilter and normalization

Metaboanalyst 5.0 was employed for matrix processing. The data was prefiltered considering QC features RSDs < 20%. Then, the data matrix was normalized by sum, log-transformed and pareto scaled. A volcano plot ($p < 0.05$, fold change >1.5) was carried out to identify down or upregulated features from HSV-1-infected-DCs at 12 and 18 hpi when compared to MOCK.[80,81] Metabolite AutoPlotter v2.6 was used to detect possible outliers and perform boxplot analysis.[71] The relevant features found were later re-evaluated through manual curation, which consists of manual reintegration of these signals, peak shape and intensity evaluation, normalization by sample protein content and statistical significance test application. Manually curated matrix was used to perform a Principal Component Analysis (PCA) to evaluate analytical performance and a volcano plot as semi quantitative analysis. Metabolite AutoPlotter v2.6 and GraphPad Prism was used to detect possible outliers and perform boxplot analysis. Interaction analysis was carried out using MetScape v3.1.3 add on in Cytoscape v3.9.1 environment.

Lipid annotation

Relevant features MS and MS/MS were obtained from raw data. Sodium formate was performed as internal calibration solution. Compass DataAnalysis 4.4.200 (Bruker) software was used to verify the molecular formula (with the smallest mass error) at relevant precursor ions (molecular adduct). The theoretical isotopic pattern was compared with the experimental isotopic pattern. The fragmentation spectra were compared to databases such as LipidBlast, LIPIDMAPS, SwissLipids and the human metabolome database (HMDB). Tools like SIRIUS and CFM-ID were employed for *in silico* fragmentation.[82–87] Nomenclature of lipids were based on guidelines proposed by Liebisch et al., 2013.[88,89] Metabolite annotation was based on the guide for annotation, quantification and best reporting practices proposed by Alseekh et al. Identification levels (A; B; C, and D) consisted of: (A) compared experimentally with a standard; (B), confident match based on MS/MS, confident match using *in-silico* MS/MS approaches and partial match based on MS/MS; (C) confident match based on MS1 and confident match using in-silico MSn approaches and partial match based on MSn; and (D) MS only.[81] Tolerance to the m/z value was set to 10 ppm. Lipidomic data were deposited in the Metabolights database under accession number MTBLS5163 and are available at the following URL https://www.ebi.ac.uk/metabolights/editor/MTBLS5163/descriptors.

Plaque-forming unit assay

The supernatant of BMDCs treated with lipid metabolism inhibitors and infected with HSV-1 strain F MOI 3 for 12 and 18 h were collected and titrated over Vero cells monolayers in flat-bottom 96 well plates with Opti-MEM (Gibco, Life Technologies). After 24 h, the plaque-forming units were screened in a ZEISS Axio Vert.1A microscope.

Western blot

Protein extract (35 μg) of treated BMDCs using RIPA buffer extraction (Cell Signaling) was run in a 12% polyacrylamide gel (BioRad) and transferred on to 0.45 mm nitrocellulose membranes. Membranes were blocked with EveryBlot Blocking Buffer (BioRad) for 5 minutes and then incubated with anti-gB clone 10B7 (1:1,000-Virusys), anti-gD clone 2C10 (1:50,000-Virusys), anti-VP16 clone 1-21 (1:1,000-Santa Cruz Biotechnology), anti-FATP2 (1:1,000-Cell Signalling), anti-DGAT2 (1:500-Santa Cruz Biotechnology), anti-CD36 (1:500-Santa Cruz Biotechnology) or HRP-anti-β-actin (1:5,000-GenScript) antibodies in EveryBlot Blocking Buffer overnight at 4°C. The membranes were washed thrice with Tris-buffered saline (TBS) and incubated with a Goat anti-mouse IgG (H+L)-HRP conjugate secondary antibody at 1:3,500 (BioRad) to detect gB, gD, VP16, DGAT2, and CD36 proteins. To detect FATP2, the goat anti-rabbit IgG HRP-conjugated secondary antibody was used at 1:2,500 dilution (GE Healthcare UK Limited). Finally, the membranes were washed thrice with TBS, revealed with ECL solution (Thermo Fisher Scientific), and analysed in a ChemiDoc Imaging Systems (BioRad). The Western blot bands were analysed using Fiji software.

Dendritic cell viability and maturation assay

BMDCs treated with lipid metabolism inhibitors and infected with HSV-1 strain F MOI 3 at 12 and 18 hpi were stained with the viability marker Zombie-Green (BioLegend), and DCs markers anti-CD11c (clone N418) and anti-I-Ab (MHC-II, clone AF6-88.5), H-2Kb (MHC-I, clone AF6-120.1), CD40 (Clone 3/23), CD80 (Clone 16-10A1), CD83 (Clone Michel-19) and CD86 (Clone GL-1) (BioLegend) for 30 minutes and washed with PBS 1X. Then, DCs were fixed with 2% PFA, acquired in a FACSVia flow cytometer (BD Biosciences) and analysed with FlowJo 10 software (BD Biosciences) (see Figure S7B).

DC migration and T cell activation *in vivo*

Spleen DCs were treated *in vitro* with 10 μM of avasimibe or lipofermata or an equivalent volume of vehicle (dimethyl sulfoxide (DMSO)) for 3 h and then infected with HSV-1 strain F MOI 3 for 1 h at 37°C. After 6 h of treatment, 5 x 10^5 treated DCs were stained with CFSE (0.5 mM) and injected into the hind limb footpads of C57BL/6 mice, as previously reported.[34] Two days later, mice were euthanized, and popliteal lymph nodes (pLNs) were surgically removed and homogenized to evaluate the presence of $CFSE^+$ DCs in these tissues using antibodies against anti-CD11c (clone N418) and anti-I-Ab (MHC-II, clone AF6-88.5) using a FACSVia flow cytometer (BD Biosciences). Alternatively, to measure the DC populations migration from the skin to infiltrating lymph nodes after HSV-1 infection, the footpads of mice were inoculated with 1x10^6 PFU of HSV-1 strain F, 10 μM of avasimibe or lipofermata and CFSE (5.6 ng). 24 h later, popliteal LN was extracted, processed, and analysed to determine the presence of $CFSE^+$ DCs using antibodies from BioLegend against CD11c (Clone N418), CD103 (clone 2E7) and CD207 (Clone 4C7). To assess T cell activation *in vivo*, mice

were simultaneously transferred with $1x10^6$ cells dye-stained virus-specific $CD4^+$ and virus-specific $CD8^+$ T cells. Popliteal LNs were extracted and processed 48 h later to analyse T cells using the following surface markers antibodies: CD4 (clone RM4-4), CD8 (clone (Ly-2), and CD25 (clone PC61) in a BD LSRFortessa X-20 (BD Biosciences) and analysed with FlowJo 10 software (BD Biosciences) (see Figures S7C and S7D).

QUANTIFICATION AND STATISTICAL ANALYSIS

RNA-seq gene set enrichment analyses

Normalized counts obtained with DEseq2 analysis were input into the GSEA software (version 4.3.2) (https://www.gsea-msigdb.org/gsea/index.jsp). The Gene Ontology database was used to find upregulated and downregulated pathways (http://geneontology.org/). Enriched pathways with false discovery rates (FDR) < 25% and nominal p-values <0.05 were considered significant. The output of this data was plotted in Cytoscape to create interaction plots based on Reactome, Gene Ontology and Wikipathways databases. RNA-seq analyses were performed with the Wald test, using the DEseq2 tool of Galaxy webserver (Galaxy.org). The Kolmogorov-Smirnov test was used for GSEA analyses.

Statistical analyses

Statistical analyses between experimental groups were assessed as indicated in the figure legends using GraphPad Prism 9 (GraphPad Software). For group comparisons, two-way ANOVA with Bonferroni multiple comparisons test was performed. Variance is reported as mean ± SEM. *$p < 0.05$, **$p < 0.01$, ***$p < 0.001$, ****$p < 0.0001$, ns: no statistical significance.